1-1-1983

The excitation of SiO in circumstellar envelopes.

Steven Emery Robinson
University of Massachusetts Amherst

THE EXCITATION OF SiO IN CIRCUMSTELLAR ENVELOPES

A Dissertation Presented

By

STEVEN EMERY ROBINSON

Submitted to the Graduate School of the
University of Massachusetts in partial fulfillment
of the requirements for the degree of

DOCTOR OF PHILOSOPHY

February 1983

Physics and Astronomy

THE EXCITATION OF SiO IN CIRCUMSTELLAR ENVELOPES

A Dissertation Presented

By

STEVEN EMERY ROBINSON

Approved as to style and content by:

David Van Blerkom

David Van Blerkom, Chairman of Committee

Robert V. Krotkov

Robert V. Krotkov Member

F. Peter Schloerb

F. Peter Schloerb Member

Nicholas Z. Scoville

Nicholas Z. Scoville Member

LeRoy F. Cook, Department Head
Physics and Astronomy

ABSTRACT

The Excitation of SiO in Circumstellar Envelopes

(February 1983)

Steven E. Robinson, B.S., Rensselaer Polytechnic Institute

Ph.D., University of Massachusetts

Directed by: Professor David Van Blerkom

The envelopes of Mira variables and VY CMa are modeled as time-independent, spherically symmetric, outflowing gas. The excitation of SiO in this environment is studied as it pertains to inversion mechanisms, using the Sobolev formalism. A new mechanism, anisotropic escape, is presented for generating ground state SiO masers, and is shown to produce luminosities comparable to those observed for $v > 0$ masers. A search for ground state maser emission produced only upper limits of $T_A^* < 1K$ for 41 late-type giant stars. This may indicate that there is a lower limit on mass loss rates for maser stars. In the models, excited vibrational state masers are found to have low luminosities. It is shown that suppression of the anisotropic escape mechanism by judicious choice of velocity law can increase the efficiency of the Kwan and Scoville radiative trapping process, and yield maser fluxes comparable to those observed. This may indicate large regions of moderate acceleration in maser star envelopes. Smoothly distributed dust shells are found to make no qualitative changes in earlier models. They do, however, suppress the anisotropic escape process within the shell cavity, resulting in increased photon fluxes

from $v > 0$ masers, and decreased fluxes from $v = 0$ masers. It is suggested that the inclusion of time-dependent outflow may alleviate some discrepancies between models and observations.

TABLE OF CONTENTS

Chapter

I. INTRODUCTION 1

Silicon Monoxide 1
Kwan and Scoville 5
Deguchi and Iguchi 7
Elitzur 9
Preliminary Discussion 10

II. THE NUMERICAL MODEL 12

Statistical Equilibrium 12
Collisional Rates 14
Sobolev Approximation 21
Physical Parameters 23
Numerical Technique 25

III. GROUND STATE MASERS 28

Anisotropic Escape 28
Numerical Results 35
Discussion 39
Summary 41

IV. EXCITED VIBRATIONAL STATE MASERS 42

Numerical Results 42
Velocity Profiles 45
Inversion Mechanisms 50
Maser Line Intensities 53
Summary 58

V. SEARCH FOR MASER EMISSION FROM THE V=0, J=1 → 0 TRANSITION OF SiO 60

Observations 60
Discussion 64

VI. RADIATIVE PUMPING OF SiO MASERS BY DUST SHELLS 67

VY Canis Majoris 67
Numerical Dust Shell Model 78
Numerical Results 83
Discussion 90
Summary 97

VII. CONCLUDING REMARKS 99

.....

BIBILIOGRAPHY 105

LIST OF TABLES

1. Peak Monochromatic Luminosities 40
2. Peak Monochromatic Luminosities 44
3. Peak Monochromatic Luminosities 55
4. Source List 62
5. Source Properties 63
6. Summary of Model Parameters 84
7. Mira Model: Peak Monochromatic Luminosities, Velocity of Peak 85
8. VY CMa Model: Peak Monochromatic Luminosities, Velocity of Peak 86

LIST OF ILLUSTRATIONS

1. The v = 1, J = 2 → 1 Transition of SiO from R Leonis 3
2. Lines of Constant ε for a Range of log τ_o 33
3. Line Profiles from the $\dot{M}$ = 2.5 x 10^{-6} $M_\odot$/yr, v_∞ = 10 km.s^{-1}, Small Star Model 38
4. The v = 2, J = 3 → 2 Profile from the Large Star, $\dot{M}$ = 1 x 10^{-5} $M_\odot$/yr Model 47
5. Schematic Diagram of Finite, Uniform Dust Shell 75
6. The v = 1, J = 3 → 2 Transition from the $\dot{M}$ = 5 x 10^{-6} $M_\odot$/yr Mira Model, with Dust Included 89

CHAPTER I

INTRODUCTION

Silicon Monoxide

The v = 1, J = 2 → 1 transition of SiO was discovered in maser emission from Orion in 1973 (Snyder and Buhl 1974), quite by accident. The spate of searches which followed soon revealed that SiO masers are frequently associated with late spectral type giant and supergiant stars, particularly Mira variables. H_2O and OH masers are almost always associated with the same sources as the SiO. The converse, however, is not true. Water and hydroxyl masers are also found near HII regions, whereas, with the possible exception of Orion, SiO maser emission is unique to cool stars.

Numerous rotational transitions of SiO are usually observed to mase in the same source. The strongest of these are the low J rotational lines of the v = 1 and v = 2 bands. The exception here is the v = 2, J = 2 → 1 transition which is seldom detectable (Olofsson et al. 1981). The ground vibrational state transitions (v = 0) are almost always nonmaser emission (e.g. Dickinson et al. 1978). In contrast to the maser lines, these are very broad, roughly parabolic, and quite weak. A typical example of an SiO maser line appears in Figure 1.

The maser nature of the SiO emission was somewhat surprising,

Figure 1. The v = 1, J = 2 → 1 transition of SiO from R Leonis (courtesy of R. Barvainis).

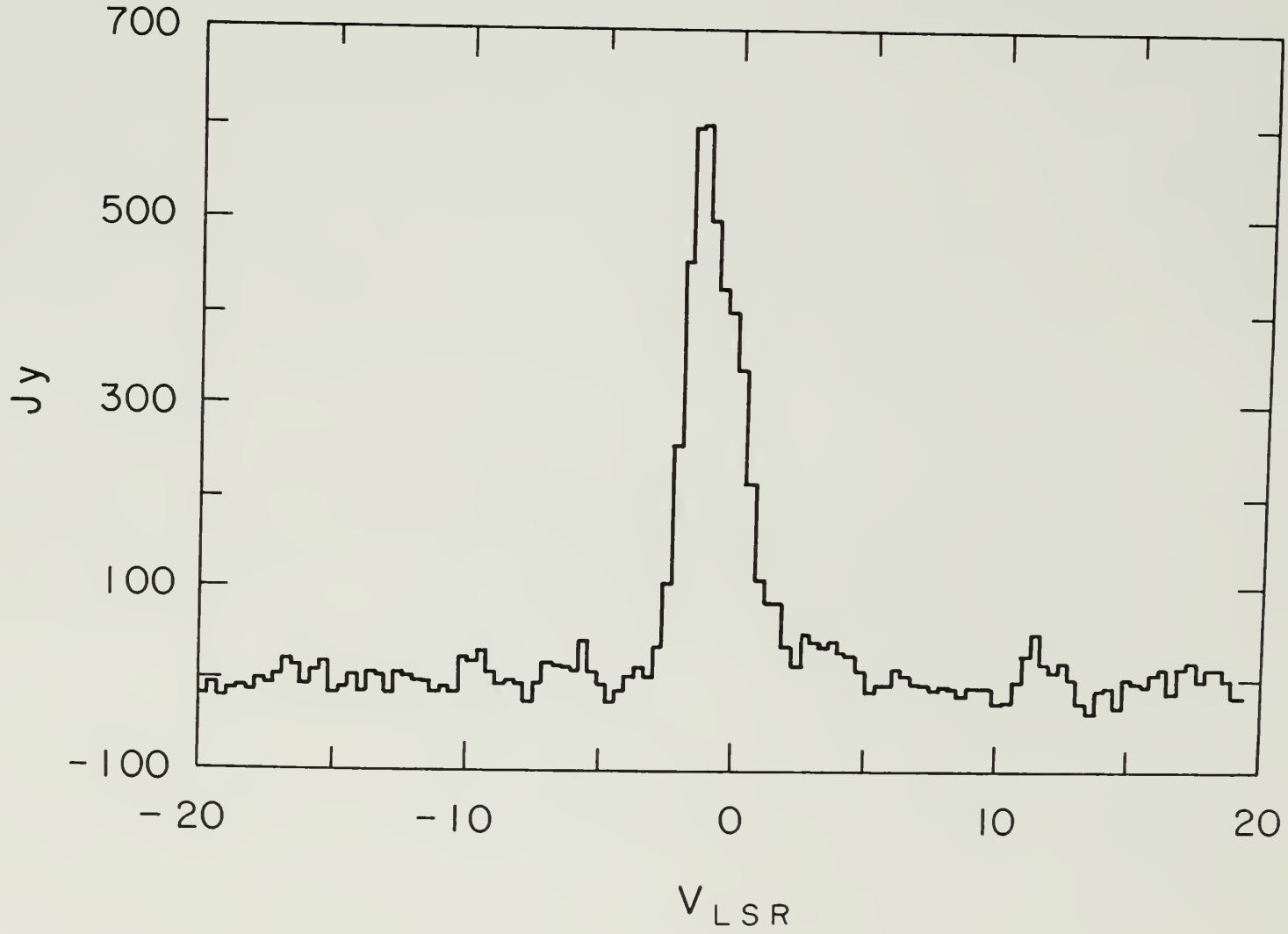
700
500
300
100
-100
Jy
-20
-10
0
10
20
V LSR

since the energy levels of SiO are so simple, especially in comparison to those of the previously known maser molecules, OH and H_2O. The richer energy structure of these molecules provides alternate branches and rates between given levels. There are, therefore, a variety of transitional routes available, which can only increase the opportunities for external conditions to drive nonthermal populations. SiO lacks such diversity.

Silicon monoxide is a simple diatomic molecule, and as such has a rotation-vibrational line spectrum. The energy of any level may be expressed as the sum of a rotational term, E_J, and a vibrational term, E_v. These are approximately

$$\begin{aligned} E_J &= h\, B_o\, J\, (J + 1), \text{ and} \\ E_v &= h\, \nu_o\, (v + 1/2)\ . \end{aligned} \tag{1}$$

J and v are the angular momentum and vibrational quantum numbers, respectively, and may take any integer value greater than or equal to zero. As usual, h is Planck's constant. The rotational and vibrational constants are roughly,

$$\begin{aligned} B_o &= 22 \text{ GHz} = 1.1 \text{ K}, \text{ and} \\ \nu_o &= 1252 \text{ cm}^{-1} = 1800 \text{ K}\ . \end{aligned} \tag{2}$$

The degeneracy of each energy level is

$$g_J = 2J + 1\ . \tag{3}$$

The selection rule for radiative transitions in simple diatomic molecules is $\Delta J = \pm 1$. This gives rise to a pure rotational spectrum within each vibrational band, the lower J transitions of which have wavelengths in the millimeter range for SiO. The vibrational lines are in the infrared, and are of two types, R and P. If the lower state has a lower J value, it is an R line. A higher J value for the bottom level implies a P line. The wavelengths for these $\Delta v = 1$ transitions are roughly 8μ for SiO.

Almost ten years have passed since the fortuitous discovery of SiO masers. A number of attempts have been made in this period to develope a useful model of these interesting sources. Despite the large body of observational data, these attempts have never been completely successful. In fact, at the time of this writing there is still no general agreement on even the mechanism which produces population inversions in SiO.

Kwan and Scoville

Kwan and Scoville (1974; hereafter KS) published one of the earlier, and more successful, models. They suggested a process that may occur in the expanding envelopes of Mira variables, whereby the populations of the higher J levels of the $v = 1$ band of SiO are selectively enhanced by high optical depths of the $v = 1 \rightarrow 0$ transitions. They also demonstrated the feasibility of their mechanism using a

numerical model for the SiO excitation.

Consider the rates of depopulation of the rotational levels of the SiO v = 1 band. If the total number density is low enough, these are dominated by emission of v = 1 → 0 photons, rather than by collisional deexcitation. If at the same time the number density of SiO molecules themselves is high enough, the v = 1 → 0 lines will be optically thick. When these lines saturate, they contain approximately the same number of photons, which means that the rate at which the v = 1 SiO deexcites via each 8μ line is uniform. Since two v = 1 → 0 transitions connect each v = 1 J level to the v = 0 band, except for the J = 0 which has only one, the depopulation rates of all but the J = 0 level are roughly the same.

Consider now the population of the v = 1 rotational levels in this same case. This may take place collisionally, predominately via v = 0 → 1. Since collisions do not obey tidy selection rules like radiation transitions, one may expect these rates to be roughly proportional to the degeneracy of each level. Alternatively, the v = 1 levels may be predominantly populated by radiative decays from the v = 2 band. If the v = 2 → 1 8μ lines are at the same time optically thin, the population rate is, again, proportional to the degeneracy. Since g_J increases with J, the higher rotational levels are populated more rapidly than the lower.

If the v = 1 levels are depopulated equally, and populated in proportion to J, one may expect a super-thermal accumulation of

population in the higher J levels, i.e. population inversions. KS showed that this process could produce maser photon emission rates of a few times 10^{43} s^{-1} from the lower J transitions of the v = 1 band of SiO from a model envelope.

There are three major drawbacks to the KS paper. The first is that their collisional rates were rather unrealistically assumed to obey selection rules similar to those of radiative transitions. The second is that they chose a value fifty times too large for the Einstein A-coefficient corresponding to the $\Delta v = 2$ transitions. Since these lines were primarily responsible for populating the v = 2 band, this choice significantly affected their calculated maser fluxes. Finally, their paper did not address in detail the question of masers in vibrational bands higher than v = 1.

Deguchi and Iguchi

Another circumstellar envelope pumping mechanism was proposed by Deguchi and Iguchi (1976; hereafter DI). Theirs is a purely radiative scheme which may take place in regions undergoing very rapid accelerations. If the mass loss of Mira variables is driven by radiation pressure on dust grains, then one can reasonably expect narrow zones of such high acceleration (e.g. Kwok 1975).

The DI anisotropic trapping mechanism hinges on the fact that, at any point in the rapidly accelerating envelope, the probability of

absorbing a stellar photon in an optically thick $\Delta v = 1$ line is larger than the probability of reradiating the same photon. If the same 8μ line were optically thin, those probabilities would, of course, be the same. The separation of the lower rotational energy states of SiO is much smaller than the excitation temperature in the envelope, so the magnetic sublevels of these are almost equally populated. Since the degeneracy increases with J, the opacities of the $\Delta v = 1$ lines, therefore, increase with J. The net result is that the relative probability of absorbing a stellar photon, compared with the probability of reradiating it, also increases with J. This leads to a pumping action on the levels of each excited vibrational band by the $\Delta v = 1$ lines joining it to the band below. DI used a numerical model, similar to that of KS, to demonstrate the validity of this process.

As with KS, there are drawbacks to the DI model. The biggest problem is that they ignored saturation effects, rendering their calculated maser luminosities useless. More basically, their mechanism can only produce emission centered on the stellar velocity, since the longest optical path lengths are tangential. Finally, one can ask if this mechanism is still important in a real envelope. DI assumed that the entire envelope undergoes rapid acceleration, but in reality only limited regions can sustain such a condition.

Elitzur

Elitzur (1980) has proposed some rather different ideas concerning SiO masers. He suggested that the masers may be located not in the circumstellar envelope, but in the stellar atmosphere itself. His paper presents arguments in favor of this hypothesis, and, naturally, points out the failings of the current envelope models. However, Elitzur has not actually presented a mechanism or a model for producing population inversions.

Elitzur's suggestions were investigated in a limited fashion by Bujarrabal and Nguyen-Q-Rieu (1981), who showed that collisional excitations of SiO dominate in the upper stellar atmosphere. They concluded that the lack of any certainty in the values of the collisional rates precluded any definite statements concerning collisional pumping of SiO masers in Mira atmospheres. They then went on to suggest a more likely process for producing high v masers in the inner envelope. Seemingly unaware of the earlier work, this process is exactly the anisotropic trapping mechanism of Deguchi and Iguchi, published five years earlier.

It is tempting to spend some time arguing the relative merits of placing SiO masers in envelope or atmosphere. Since VLBI observations show at least the v = 1 masers scattered over regions of several stellar radii in some sources (Lane 1982), the envelope models that we have chosen to investigate are still significant, regardless of the

merits of Elitzur's hypothesis.

Preliminary Discussion

When we began this research, we felt that the full potential of spherically symmetric, time-independent, expanding envelope models had not yet been determined. The obvious areas needing improvement were those enumerated for the earlier envelope maser models. That is to say, one must use accurate radiative rate coefficients, reasonable collisional rates, and a larger number of SiO energy levels in the statistical equilibrium calculations. In addition, important physical aspects of the circumstellar envelope had been inadequately treated. The first of these is, of course, the velocity structure. Another is the infrared radiation from the dust shells, which dominates the continuum from Mira variables at wavelengths near 8μ.

We attempted to make our model more accurate, more complete, and without bias concerning the earlier work. By so doing we could not only confirm these mechanisms, but also examine their interplay and relative importance. In addition, we could also look for other types of inversion mechanisms, which may have been missed.

The examination of theoretical maser mechanisms is interesting in and of itself, but one should not lose sight of the larger goal of such research. This is, of course, the development of models which will allow observations of SiO masers to be used to probe the physical

conditions of the maser sources, themselves. To this end, we have more fully explored the limitations and strengths of this particular class of model. As a result, we can offer some promising suggestions for the directions that the next generation of SiO maser models should go.

CHAPTER II

THE NUMERICAL MODEL

Statistical Equilibrium

We have assumed that the SiO molecules are in statistical equilibrium in order to determine the energy level populations. This implies that the level populations are constant in time, having the number leaving each state exactly balancing the number entering. The rate of molecules entering some level i from levels j, having lower energies, is

$$\sum_{j=1}^{i-1} n_j \left(B_{ji} J_{ij} + C_{ji}\right) , \text{ where}$$

n_j is the population of energy level j, B_{ji} is the Einstein coefficient for absorption, J_{ij} is the radiation field at the frequency of the transition from j to i, and C_{ji} is the collisional excitation coefficient. The rate for entering i from levels above is

$$\sum_{j=i+1}^{\infty} n_j \left(A_{ji} + B_{ji} J_{ji} + C_{ji}\right) ,$$

where A_{ij} and B_{ji} are the Einstein coefficients for spontaneous emission and stimulated emission, respectively, and C_{ji} is the collisional deexcitation coefficient. The rate at which molecules leave i for lower levels j is

$$\sum_{j=1}^{i-1} n_i \, (A_{ij} + B_{ij} \, J_{ij} + C_{ij}) \ , \text{ and}$$

the number leaving for higher levels is

$$\sum_{j=i+1}^{\infty} n_i \, (B_{ij} \, J_{ij} + C_{ij}) \ .$$

For each level i, we, therefore, have

$$\sum_{j=1}^{i-1} [n_j \, (B_{ji} \, J_{ji} + C_{ji}) - n_i \, (A_{ij} + B_{ij} \, J_{ij} + C_{ij})]$$

$$+ \sum_{j=i+1}^{\infty} [n_j \, (A_{ji} + B_{ji} \, J_{ji} + C_{ji}) - n_i \, (B_{ij} \, J_{ij} + C_{ij})] = 0 \ . \qquad (1)$$

For N_ℓ levels included in the calculation, this yields N_ℓ equations with N_ℓ unknowns (the n_i). We replace the equation for the highest level, $i = N_\ell$, with the requirement of number conservation

$$\sum_{i=1}^{N_\ell} n_i = N_t \ , \text{ where } N_t \qquad (2)$$

is the total number of molecules in the included levels. For a level ℓ and another of higher energy u

$$A_{u\ell} = B_{u\ell} \, 8\pi h\nu^3/c^3 \ , \text{ where} \qquad (3)$$

ν is the frequency of the transition, and

$$B_{\ell u} = B_{u\ell} \, g_u/g_\ell \ . \qquad (4)$$

The g_i are, as before, the degeneracies.

Since SiO is a simple diatomic molecule, transitions may be described by changes of angular momentum and vibrational quantum numbers from J and v to J' and v'. For pure rotational transitions

$$A\ (J \rightarrow J') = (64\pi^4\ \nu^3\ \mu^2/3hc^3)\ (J' + 1)/(2J' + 3)\ , \qquad (5)$$

where μ is the electric dipole moment, and J' refers to the lower state. For vibrational transitions

$$A\ (J\ v \rightarrow J'\ v') = A\ (v \rightarrow v')\ S_J/(2J + 1)\ , \text{ where}$$

$$S_J = J + 1 \text{ for } J' = J + 1\ , \qquad (6)$$

$$S_J = J \text{ for } J' = J - 1\ , \text{ and}$$

J refers to the upper state. We have taken the values for the $A\ (v \rightarrow v')$ from Hedelund and Lambert (1972) in our early models, and those of Tipping and Chackerian (1981) for the later ones. These two sets of numbers differ only slightly for the smaller values of Δv.

Collisional Rates

The collisional rates C_{ij} are far more difficult to determine than the radiative rates. Rates for total collisional excitation between vibrational bands can be measured in the laboratory. To separate the intrinsic properties of the rates, we may write

$C_{ij} = N_H K_{ij}$, where

N_H is the total number density. Based on data taken by Milikan and White (1963), Lifshitz (1974) found that simple systems are adequately described by

$$K\ (T,\ v = 1 \rightarrow 0) = 3.03 \times 10^6\ \theta^{2.66}\ \mu^{2.06} \cdot \exp\ (-0.492\ \theta^{0.681}\ \mu^{0.302}\ T^{-1/3})\ cm^3.s^{-1}\ mole^{-1} \quad (7)$$

where $\theta = 1.48\ (\omega_e - 2\omega_e\ x_e)$, and μ is the reduced mass of the colliding system. ω_e and x_e are empirically determined parameters that we have taken from Manson et al. (1977). Lifshitz states that errors of ± 50% should be expected from the above expression. For SiO - H_2 collisions this becomes

$$K\ (T,\ v = 1 \rightarrow 0) = 8.53 \times 10^{-9} \cdot \exp\ (-9.8 \times 10^1\ T^{-1/3})\ cm^3.s^{-1}\ . \quad (8)$$

One may obtain rates for other Δv transitions from the expression,

$$K\ (T,\ v \rightarrow 0) = K\ (T,\ v = 1 \rightarrow 0)\ (E_v/E_1)^{3/2} \cdot \exp[-(E_v/E_1 - 1)]\ , \quad \text{(Elitzur 1980)} \quad (9)$$

where the E_i are the appropriate vibrational energies.

Unfortunately, these rates concern only the vibrational levels; that is to say, they contain no information about the J structure of the transitions. State to state rates cannot yet be measured, and until recently, could only be computed for temperatures much lower

than those of circumstellar envelopes. We have, therefore, assumed that the pure rotational rates have the form

$$K(T, J_u \to J_\ell) = K_o (hB_o/kT)^{1/2} (g_\ell/g_u) \cdot [1 - \exp(-kT/\Delta E_{u\ell})] F(J_u, J_\ell) \text{ , where} \quad (10)$$

$$F(J_u, J_\ell) = 1 + (J_u - J_\ell)/[1 + (\Delta J - 2)^2] \text{ .}$$

As usual, g is the degeneracy, and B_o is the rotational constant for SiO.

At low temperatures, $K(T, J_u \to J_\ell) \propto T^{1/2}$, implying that the cross-sections for collisional transitions are roughly constant in T. At high temperatures $K(T, J_u \to J_\ell) \propto T^{-1/2}$, indicating a T^{-1} dependence for the cross-sections. Goldreich and Kwan (1974) have suggested this temperature dependence, which has a rather intuitive justification. At low temperature, the kinetic energy of the average colliding molecule is less than all but the lowest energy transitions; therefore, only a fixed number of states are accessible, and only the energy of the collisions ($\propto T^{1/2}$) affects the rates. At high temperature, on the other hand, the kinetic energy is larger than most transitions; therefore, any increase in temperature increases the number of accessible states. One might, therefore, expect the cross-section for a transition to any single state to decrease with increasing T.

Green and Chapman (1978) have calculated rotational collisional rates for CO - He collisions at temperatures $\lesssim$ 100K. Using a value of

$K_o = 1.86 \times 10^{-10}$ cm $^3.s^{-1}$, a comparison of their calculated rates to our values gives an average difference of 25% at 20K, 20% at 50K, and 15% at 100K. Even the largest individual discrepancies in these cases are not much more than a factor of two different.

Encouraged by such good agreement, we have used this formula for the collisional rates in our model. We have taken $K_o = 2.8 \times 10^{-10}$ $cm^3.s^{-1}$ because of the different reduced mass for SiO - H_2 collisions. At 1500K, this gives a typical pure rotational rate of 10^{-11} $cm^3.s^{-1}$.

Collisional rates for downward transitions between the vibrational bands are assumed to be proportional to those for the rotational transitions. K_o, the constant of proportionality, can then be determined since the individual state to state rates must sum to the previously given vibrational rates. If the total number of all molecules is N_H, the number of SiO molecules in a given vibrational band is n (v), and the number in any state is n (v, J), then

$$N_H \, n\,(v)\, K\,(T,\ v \to 0) = N_H \sum_f \sum_i n\,(v,\ J_i)\, K\,(T,\ vJ_i \to 0\ J_f)\ . \tag{11}$$

Since n (v, J = 0) = n (v)/U_R (T), where U_R (T) is the rotational partition function, and

$$n\,(v,\ J) = n\,(v,\ J = 0)\,(g_J/g_o)\,\exp\,[-E\,(J)/kT]\ , \tag{12}$$

we obtain the sum rule

$$K\,(T,\ v \to 0)\ U_R\,(T) = \sum_f \sum_i g_i\ K\,(T,\ vJ_i \to v = 0\ J_f)\ \exp\,[-E\,(J_i)/kT]\ . \qquad (13)$$

Finally, all transitions with the same J_f, J_i, and Δv are assumed to be equal. A typical value at 1500K for $\Delta v = 1$ would be roughly 10^{-14} $cm^3.s^{-1}$. Upward rates are computed from detailed balance.

Very recently Bienick and Green (1982; hereafter BG) calculated high temperature rotational rates for SiO. These are about an order of magnitude larger than ours, and have a roughly $T^{1/2}$ dependence. This implies that the BG cross-sections are essentially constant at high temperatures.

If inversions are to be produced by radiative transitions between vibrational bands, as suggested by most mechanisms, including Elitzur's, these radiative transitions must take place on time scales much shorter than those of the collisional transitions. Therefore, assuming the maximum possible radiative decay rate,

$$n\,(v,\ J)\ N_H\ K\,(T,\ vJ \to v'\ J') \ll n\,(v,\ J)\ A\,(vJ \to v'\ J')\ , \text{ or} \qquad (14)$$

$$N_H\ K\,(T,\ vJ \to v'\ J') \ll A\,(vJ \to v'\ J')\ .$$

A typical value of A is 5 s^{-1}, and a typical value of K from BG is about 10^{-10} $cm^3.s^{-1}$. Therefore, N_H must be significantly less than 10^{10} cm^{-3} for inversions to occur by radiative decays. For a time-independent outflow, the number density is given by

$N_H = \dot{M}\ [4\pi\ r^2\ v(r)\ m_{H2}]^{-1}$, where

$\dot{M}$ = mass loss rate,

v(r) = velocity of the flow,

and m_{H2} = H_2 molecular mass. (15)

Taking reasonable values of $10^{-5}\ M_\odot/yr$ and 5 $km.s^{-1}$ for $\dot{M}$ and v, respectively, we find that the number density constraint forces the masing region to be more than 6×10^{13} cm (about two stellar radii) from the center. This is unsettling since SiO must be restricted to a few stellar radii, even in envelope models. It is certainly fatal for Elitzur's photospheric model, since number densities in the stellar atmosphere are well above $10^{10}\ cm^{-3}$ regardless of the mass loss rate.

A more serious contradiction arises when one considers the optical depths of the SiO vibrational lines, which are directly related to the SiO number density. To produce population inversions in a given vibrational band, the 8μ lines connecting it to the band below must be optically thick. In the Sobolev formalism (Castor 1970, Mihalas 1978) the optical depth is

$\tau = \tau_o\ [1 - \mu^2\ (\varepsilon - 1)]^{-1}$, and

$\tau_o = \chi\ (r)/(V/r)$

r = distance from center (16)

V = velocity in units of the thermal velocity

χ = line center opacity

$$= B_{\ell u}\, n_\ell \left[1 - (g_\ell\, n_u / g_u\, n_\ell)\right] (h\nu / c\Delta\nu_D)$$

for a lower state ℓ and an upper state u. ν and $\Delta\nu_D$ are the line frequency and Doppler width, respectively. μ and ε are both of order unity. Assuming thermal equilibrium, the constraint

$\tau_o \gg 1$, implies

$$fN_H \gg U(T) \left[1 - \exp(-\Delta E_{u\ell}/kT)\right]^{-1} \cdot \exp(\Delta E_{u\ell}/kT)\, v/(rhB_{\ell u}\, g_\ell) \,. \qquad (17)$$

Here, f is the number fraction of SiO molecules in the envelope, U (T) is the partition function, and $\Delta E_{u\ell}$ is the energy separation.

Since v = 2 SiO masers are routinely observed, let us consider a line from v = 2 to v = 1. Assume the following reasonable values:

$v = 5$ km.s^{-1} ,

$r = 6 \times 10^{13}$ cm ,

and T = 1500K.

We find that the limit on the SiO number density becomes

$fM_H \gg 4 \times 10^5$ cm^{-3} .

Choosing a value of $f = 3 \times 10^{-5}$, optimistically corresponding to about half of the silicon being in SiO, the total number density is constrained,

$$N_H >> 1 \times 10^{10} \text{ cm}^{-3} .$$

Since the BG rates seem to require number densities less than 10^{10} cm^{-3} to allow inversions, we have arrived at a contradiction. All of our work had been completed by the time the BG rates became available to us. Considering the contradiction that arises with them, we chose not to try to incorporate them into our models at present.

Sobolev Approximation

We have used the large velocity gradient (LVG) or Sobolev approximation for computing the radiation field in our model envelope. The basic premise of the approximation is that in a spherical expanding medium, the velocity field decouples the material at each radius from the rest of the gas. Since any region may interact with another only through the emission and absorption, in this case, of line photons, they become independent once the velocity along the line between them exceeds the thermal Doppler velocity. In the limiting case of an expansion velocity much larger than thermal, the radiative transfer reduces to a completely local problem. One may then write

the radiation field as

$$J(r) = (1 - \bar{\beta})\, S(r) + \beta_c(r)\, I_* \,. \tag{18}$$

$S(r)$ is the local source function, and I_* is the continuum radiation density contributed by the core (the stellar photosphere). β is the probability, averaged over frequency and angle, that a photon may escape the local region. β_c is a similar quantity, averaged only over the solid angle of the continuum source. The escape probability in any given direction is just

$$\beta(r, \mu) = [1 - \exp(-\tau(r, \mu))]/\tau(r, \mu) \,, \tag{19}$$

where $\tau(r, \mu)$ has the same definition as given earlier. This leads to

$$\bar{\beta}(r) = \chi(r)^{-1} \int_0^1 [1 - \exp(-\chi/Q(r, \mu)]\, Q(r, \mu)\, d\mu \,, \tag{20}$$

and

$$\beta_c(r) = \chi(r)^{-1} \int_{\mu_c}^1 [1 - \exp(-\chi/Q(r, \mu)]\, Q(r, \mu)\, d\mu \,, \tag{21}$$

$$Q(r, \mu) = 1 + \mu^2(\varepsilon - 1) \,, \text{ and} \tag{22}$$

$$\mu_c = [1 - (r_c/r)^2]^{1/2} \,. \tag{23}$$

μ is the direction cosine of the angle to the center, and

$$\varepsilon = d(\ell n\, V)/d(\ell n\, r) \,. \tag{24}$$

This formalism also allows the easy computation of line profiles.

After conversion from energy density to intensity, the emergent flux is

$$F(x) = 2\pi \int_{r_c}^{\infty} S(r_o)\,[1 - \exp(-\tau(-\infty, p, x))]\,p\,dp$$

$$+2\pi \int_{o}^{r_c} S(r_o)\,[1 - \exp(-\tau(-\infty, p, x))\,\Phi(x_c)]\,p\,dp \qquad (25)$$

$$+2\pi\, I_* \int_{o}^{r_c} [\exp(-\tau(-\infty, p, x)\,\Phi(x_c)]\,p\,dp\ .$$

As usual, p is the impact parameter, and

$$x = |\nu_o - \nu|/\nu\ .$$

$\Phi(x_c)$ is zero for $x < 0$ and 1 for $x > 0$, accounting for occultation by the core.

Physical Parameters

Assuming a steady-state outflow of matter from the star, matter conservation gives the number density at every radius directly from the flow velocity. In our early work, we used two velocity laws:

$$v(r) = v_o\,(r/R_*)^{\epsilon}\ , \text{ and}$$

$$v(r) = v_\infty\,[1 - R_*/r]^{1/2}\ . \qquad (26)$$

R_* is the stellar radius. The second law approximates a radiatively

driven flow, and is similar to that suggested by Reimers (1977). In this law,

$$\varepsilon\ (r) = [2\ (r/R_* - 1)]^{-1}\ . \tag{27}$$

The kinetic temperature is assumed to follow a relationship similar to that for an adiabatic expansion,

$$T_k\ (r) = T_o\ (r/R_*)^{-1/2}\ . \tag{28}$$

Since the star is represented by a blackbody of temperature T_*, either 2000K or 2700K, one might expect to choose $T_o = T_*$. One can, however, simplify the calculation by using a somewhat lower value.

The reason for our choice of T_o lies in the nature of the statistical equilibrium calculation. The only way in which levels not explicitly included affect the model is through the partition function. We have used the approximation given by Townes and Schawlow (1955):

$$U\ (T) = \exp\ (-h\omega_e/2kT) \cdot [1 - \exp\ (-h\omega_e/kT)]^{-1}\ kT/hB_o\ . \tag{29}$$

ω_e is the vibrational constant, and B_o is the rotational constant. In thermal equilibrium, the population of any level is

$$n_i^* = N_{SiO}\ g_i\ \exp\ (-\Delta E_{io}/kT)/U\ (T)\ . \tag{30}$$

N_{SiO} is the total number of SiO molecules per unit volume. The number of molecules in the number constraint, N_t, is the sum of the n_i^* over the included states, and is significantly less than N_{SiO}. Strictly speaking, this is incorrect since radiative cooling causes the excitation temperature to always be lower than the kinetic temperature. Ideally, one would fit for a value of T_x, and use that value in the partition function. In our case, this proved to be too time-consuming. To account for the effect in an easier way, we set T_o equal to an artificially low value, either 1000K or 1600K, and assumed kinetic and excitation temperatures to be equal.

Near the photosphere of Mira variables where the temperature is relatively high, the tenacious SiO molecule is probably the dominant silicon bearing compound (e.g. Tsuji 1973). At some radius, the envelope becomes cool enough for dust grains to form, incorporating a large portion of the silicon. Since most maser action takes place within a few stellar radii of the center, it is probably interior to the majority of the dust shell (e.g. Deguchi 1980). We have, therefore, adopted a constant number fraction of SiO, 3×10^{-5}, corresponding to about half of the silicon being in this compound.

Numerical Technique

Usually each model includes the lowest 7 rotational levels in each of 4 or 5 vibrational bands of SiO. This means that 28 or 35

equations most be solved simultaneously. To complicate matters, the presence of the radiation field term makes these equations highly non-linear. To solve these at each radial point, we have used a modified form of the Newton-Raphson method. This is a linearization based on a Taylor's expansion. To find a solution vector $\underline{x}$ such that

$\underline{\underline{f}}\ (\underline{x}) = \underline{0}$, one expands,

and retains only the first derivative term,

$$\underline{\underline{f}}\ (\underline{x}) \simeq \underline{\underline{f}}\ (\underline{x}_o) + \underline{\underline{f}}_x\ (\underline{x}_o)\ \Delta\underline{x} \simeq \underline{0} \ .$$

Here $\underline{\underline{f}}_x\ (\underline{x}_o)$ is the Jacobian matrix evaluated at some approximate solution $\underline{x}_o$. $\Delta\underline{x}$ is the change in $\underline{x}_o$ needed to produce a closer approximation to the actual $\underline{x}$. Any desired accuracy in $\underline{x}$ may be found, in principle, by iteration of this process. Convergence properties of the Newton-Raphson method are very good if the initial guess is, in some sense, close to the correct solution.

In a maser problem, the radiation field behaves exponentially once the populations invert. This can cause the initial guess of populations to be quite different from the actual solution. In such a situation, the convergence of the Newton-Raphson method is often very poor. What frequently happens is that, in some step, the increment to the solution is badly overestimated, resulting in a new solution vector which is worse than the old one. Once this occurs, convergence is seldom obtained.

To lessen the severity of this problem, we have made a simple addition to the numerical technique. In effect it decouples the equations, and reduces the increment size if an iteration fails to improve a solution. This is done by multiplying the diagonal of the Jacobian matrix by a factor which increases if the solution fails to improve. If the solution improves with a step, the factor decreases until the normal Newton-Raphson is re-established.

Each rate equation should equal zero if the exact solution is found. There is, of course, always a residual in reality. We normalize this by the largest term in the equation, and use the result as a test for convergence and correctness of solution. The solution is considered acceptable if all residuals are less than 10^{-7} and the last step changed the populations by no more than 0.1%.

CHAPTER III

GROUND STATE MASERS

Anisotropic Escape

Perhaps the most interesting results from our model are those concerning a mechanism capable of producing strong masers in the ground vibrational state ($v = 0$) of SiO. We are not the first to note $v = 0$ inversions in a numerical model. It was briefly mentioned by Kwan and Scoville (1974) in their paper on radiative trapping, leading to inversions in the $v = 1$ vibrational state. Their explanation of the ground state maser is based on the fact that the radial optical depth, $\tau\ (r,\ \mu = 1)$, can be significantly larger than the average optical depth,

$$\bar{\tau}\ (r) = 1/2 \int_{-1}^{1} d\mu\ \tau\ (r,\ \mu)\ , \tag{1}$$

so that the former is optically thick, and the latter is optically thin. This follows from Equation (II.16) if $0 < \varepsilon < 1$. For an optically thick transition, $\beta\ (r,\ \mu) \simeq 1/\tau\ (r,\ \mu)$, while for a thin transition, $\beta\ (r,\ \mu) \simeq 1$. The rate at which molecules are removed from a ground state rotational level by absorption of stellar photons is

$$R_\ell = (n_\ell\ B_{\ell u} - n_u\ B_{u\ell})\ \beta_c\ (r)\ I_* \ . \tag{2}$$

As before, I_* is the stellar radiation field, and $B_{\ell u}$ and $B_{u\ell}$ are the Einstein rates of absorption and stimulated emission, respectively. In terms of these parameters the optical depth is

$$\tau\ (r,\ \mu) = (h/4\pi)(rc/V)(n_\ell\ B_{\ell u} - n_u\ B_{u\ell})/[1 + \mu^2\ (\varepsilon - 1)]\ , \qquad (3)$$

where ε retains the definition of Equation (II.24).
Thus, for an optically thick line, using the asymptotic form of $\beta_c\ (r)$, we have

$$R_\ell = (2\pi\varepsilon V/hrc)\ I_*\ (1 - \mu_c) \qquad (4)$$

which is a constant at any value of radius. In this case, the rate at which the v = 0 rotational levels are depleted depends on the number of radiative excitation routes available to them. The inverse process, involving spontaneous emission, depends on the angle averaged optical depth $\bar{\tau}\ (r)$, which by hypothesis is less than unity. Thus, radiative processes populate the ground rotational levels at rates not necessarily proportional to the number of available routes, and population inversions may occur.

In the myriad of competing radiative and collisional processes which set the level populations, it is often difficult to separate out one mechanism and claim that it is the one responsible for a given effect. The process described above is not free of objection. For one thing, the asymptotic forms $\bar{\beta}\ (r) = 1$ and $\beta_c\ (r) = 1/2\ (1 - \mu_c)$. $\varepsilon/\tau_o\ (r)$ are not clearly applicable for the spontaneous and induced

radiative transitions, respectively. KS used a velocity law of the form $V(r) \propto r^{\varepsilon}$ with $\varepsilon = 0.2$, and obtained weak ground state maser emission. In this case the radial optical depth $\tau(r, \mu = 1)$ is only three times the angle averaged optical depth $\bar{\tau}(r)$, so that the induced transitions will hardly be saturated if the spontaneous transitions are optically thin. If one nevertheless assumes the mechanism to work, then there is only one radiative excitation route available to the $v = 0$, $J = 0$ level, namely that to $v = 1$, $J = 1$ (if one, for simplicity, ignores higher vibrational levels). All other $v = 0$, J levels have two routes which are permitted to $v = 1$, $J \pm 1$. It will thus be very difficult to invert the $v = 0$, $J = 0$ and $J = 1$ levels, so that one would expect any ground state maser emission to be in transitions other than the $J = 1 \rightarrow 0$ line. In their numerical model, however, it is the $J = 1 \rightarrow 0$ line that is inverted.

Deguchi and Iguchi (1976) proposed an infrared pumping scheme for vibrationally excited SiO masers which involved an anisotropic trapping process. They showed that this process was effective in producing inversions of the $v \geq 1$ populations in a region of the outflow where very rapid acceleration of the material occurs ($\varepsilon \approx 5$). We suggest here that a complementary process, which we term anisotropic escape, can produce inversions of the $v = 0$ populations of SiO in a region of very gradual acceleration. This effect could be responsible for the Kwan and Scoville results, since they assumed $\varepsilon = 0.2$. In addition, it is suggested that anisotropic escape limits the radial

extent of any such region of the outflowing envelope where v = 1 masers may exist.

The probability of a photon escaping from a point along a radial path in

$$\beta_* (r) = [1 - \exp (-\tau_o/\varepsilon)] (\tau_o/\varepsilon) . \qquad (5)$$

We can express anisotropic escape by the ratio $\bar{\beta} (r)/\beta_* (r)$, i.e. the ratio of the probabilities of escape from a region of the envelope and of absorption of a stellar photon in the same region. For an optically thin line ($\tau_o << 1$), the asymptotic forms of $\bar{\beta}$ and β_* are unity, so $\bar{\beta}/\beta_* = 1$. For an optically thick line ($\tau_o >> 1$)

$$\beta (r, \mu) \to 1/\tau (r, \mu) = [1 + \mu^2 (\varepsilon - 1)]/\tau_o (r) , \text{ so}$$

$$\beta_* (r) \to \varepsilon/\tau_o (r) , \text{ and}$$

$$\bar{\beta} (r) \to [1 + (\varepsilon - 1)/3]/\tau_o (r) .$$

Therefore,

$$\bar{\beta}/\beta_* = (2 + \varepsilon)/3\varepsilon \qquad (\tau_o >> 1) \qquad (6)$$

(cf. Equation (3) of Deguchi and Iguchi 1976). For $\varepsilon = 0.2$, for example, $\bar{\beta}/\beta_*$ varies from unity at $\tau_o = 0$ to 3.67 as $\tau_o \to \infty$. Figure 2 shows the behavior of $\bar{\beta}/\beta_*$ over a wide range of τ_o and for several values of ε.

At the temperatures within a stellar envelope, roughly equal

Figure 2. Lines of constant ε for a range of log τ_o.

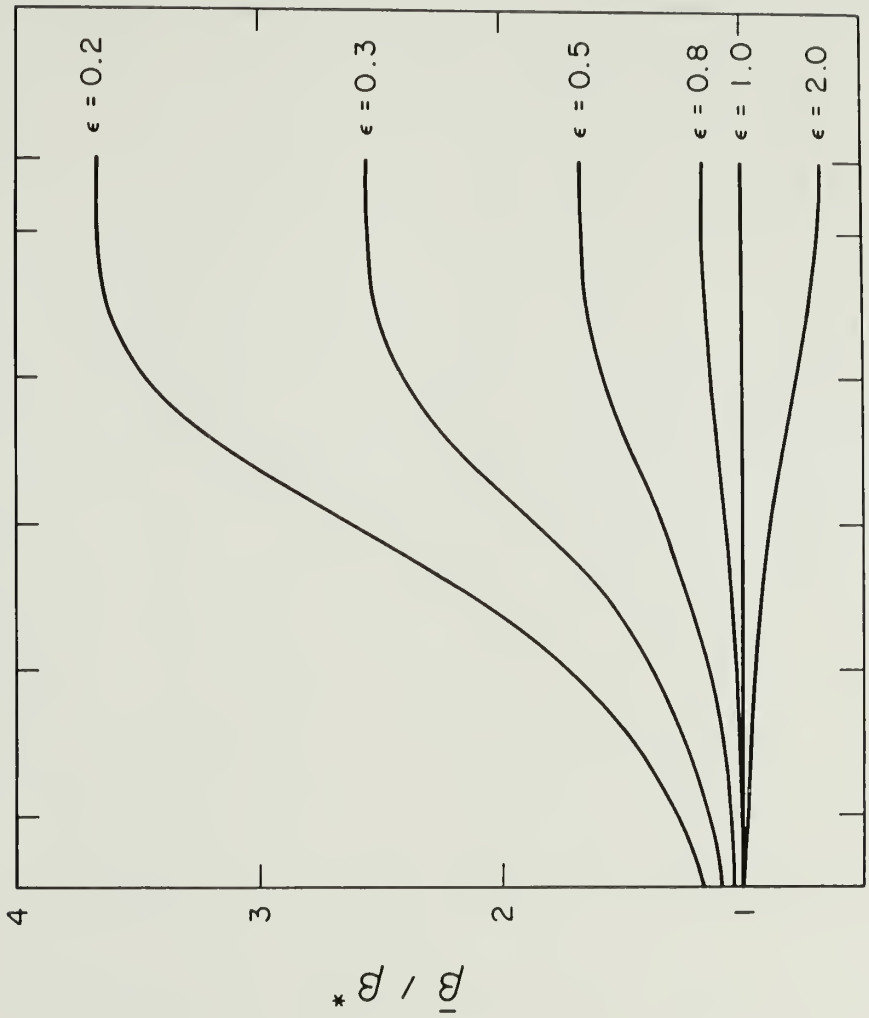
ε = 0.2
ε = 0.3
ε = 0.5
ε = 0.8
ε = 1.0
ε = 2.0
4
3
2
1
-1.0 -0.8 -0.4 0 0.4 0.8 1.0
log τ0
β1 / β*

populations of the magnetic sublevels of a given vibrational band will be established. The opacity (and thus τ_o) of each $v = 1 \rightarrow 0$ transition will therefore increase with the degeneracy, $g_J = 2J + 1$, of the lower rotational level of the transition. In other words, as the J value of the $v = 0$ levels increase, $\log \tau_o$ moves to the right along a curve of constant ε in Figure 2. Hence, in a region of slow acceleration, where $\varepsilon < 1$, $\bar{\beta}/\beta_*$ also increases with J. As the figure shows, the changes in $\bar{\beta}/\beta_*$ are most rapid in the vicinity of $\tau_o = 1$.

Let us now consider what happens to the populations of the higher J levels of $v = 0$ under these circumstances. Since β_* decreases with J, stellar photons have more difficulty penetrating to a given region and causing excitation. Conversely, the photons from the resulting decays of this excitation escape from the region relatively more readily (larger $\bar{\beta}/\beta_*$) rather than causing additional local excitation. As one moves to lower values of J, the opposite situation is encountered, whereby stellar photons more easily reach a given radius, but find it relatively more difficult to escape. For $\tau_o \sim 1$ and $\varepsilon < 1$, and if there are many stellar photons present, the net result is the selective depopulation of the lower J, $v = 0$ levels. Since these radiative transitions terminate predominantly in the lower J, $v = 1$ levels, the process also selectively populates these levels. Under such conditions, population inversions occur in the ground vibrational state, while inversions in the $v = 1$ band are suppressed. The next section illustrates the functioning of this process in the

context of our numerical model of an expanding envelope around a late-type giant star.

Numerical Results

The model computations confirm that anisotropic escape does produce inversions of the v = 0 populations, which under certain conditions are substantial. These inversions never occur beyond a few stellar radii of the center, and are strongest, as expected if anisotropic escape is the dominant mechanism, where τ_o for the $v = 1 \rightarrow 0$ lines is of order unity. Inversions persist, however, when the $v = 1 \rightarrow 0$ optical depths are as large as five or six. Since the Kwan and Scoville mechanism for ground state maser emission requires $\tau_o < 1$, this fact excludes that explanation for the existence of inverted populations. An interesting result is that strong v = 1 maser emission is seen only when the v = 0 rotational transitions are entirely nonmaser.

The v = 0 nonmaser lines are practically uniform in appearance, i.e. roughly parabolic, centered at zero velocity and extending over the entire velocity range from $-v_\infty$ to $+v_\infty$. This agrees with the observed profiles. Compared to the maser emission, the dominant contribution to the nonmaser lines arises from larger radii. The calculations presented here are based on a model envelope terminated at a value approximately ten times the stellar radius. The maser

lines are already entirely formed within this region, but the nonmaser lines, which are generally very optically thick, will have their emission artificially truncated. Compare this calculation with that of Morris and Alcock (1977), in which the nonmaser SiO emission is found to peak beyond 5×10^{16} cm, or roughly 1000 stellar radii. It is not, therefore, surprising that the intensities we compute for the nonmaser transitions are significantly lower than those observed. We have, however, run one model out to much larger radii. We find the maser lines unchanged, as expected, but the intensities of the nonmaser lines are greatly increased while their profiles are affected only little.

In sharp contrast to the nonmaser lines, the maser transitions are characterized by narrow (1.5 to 3 $km.s^{-1}$) spikes at a velocity intermediate to zero and $-v_\infty$. These are actually the short-wavelength components of pairs of lines formed in the near and far hemispheres of the envelope. The long-wavelength components are occulted by the stellar disk. Frequently, the less intense lines show a weak "pedestal" of emission extending from the velocity of the shortward spike to the velocity of the occulted longward spike. Figure 3 gives examples of both maser and nonmaser profiles for the small star model with $\dot{M} = 2.5 \times 10^{-6}$ $M_\odot/yr$. The terminal velocity $v_\infty = 10$ $km.s^{-1}$ and the fractional abundance of SiO is $f_{SiO} = 3 \times 10^{-5}$. In Figure 3a the maser line shown is that of the $v = 0$, $J = 2 \rightarrow 1$ transition and displays the shortward displaced spike and pedestal emission. Figure 3b

Figure 3. Line profiles from the $\dot{M} = 2.5 \times 10^{-6}\ M_{\odot}/yr$, $v_{\infty} = 10\ km.s^{-1}$, small star model.

Part a: the v = 0, J = 2 → 1 transition, a typical maser line.

Part b: the v = 0, J = 3 → 2 transition, a typical nonmaser line.

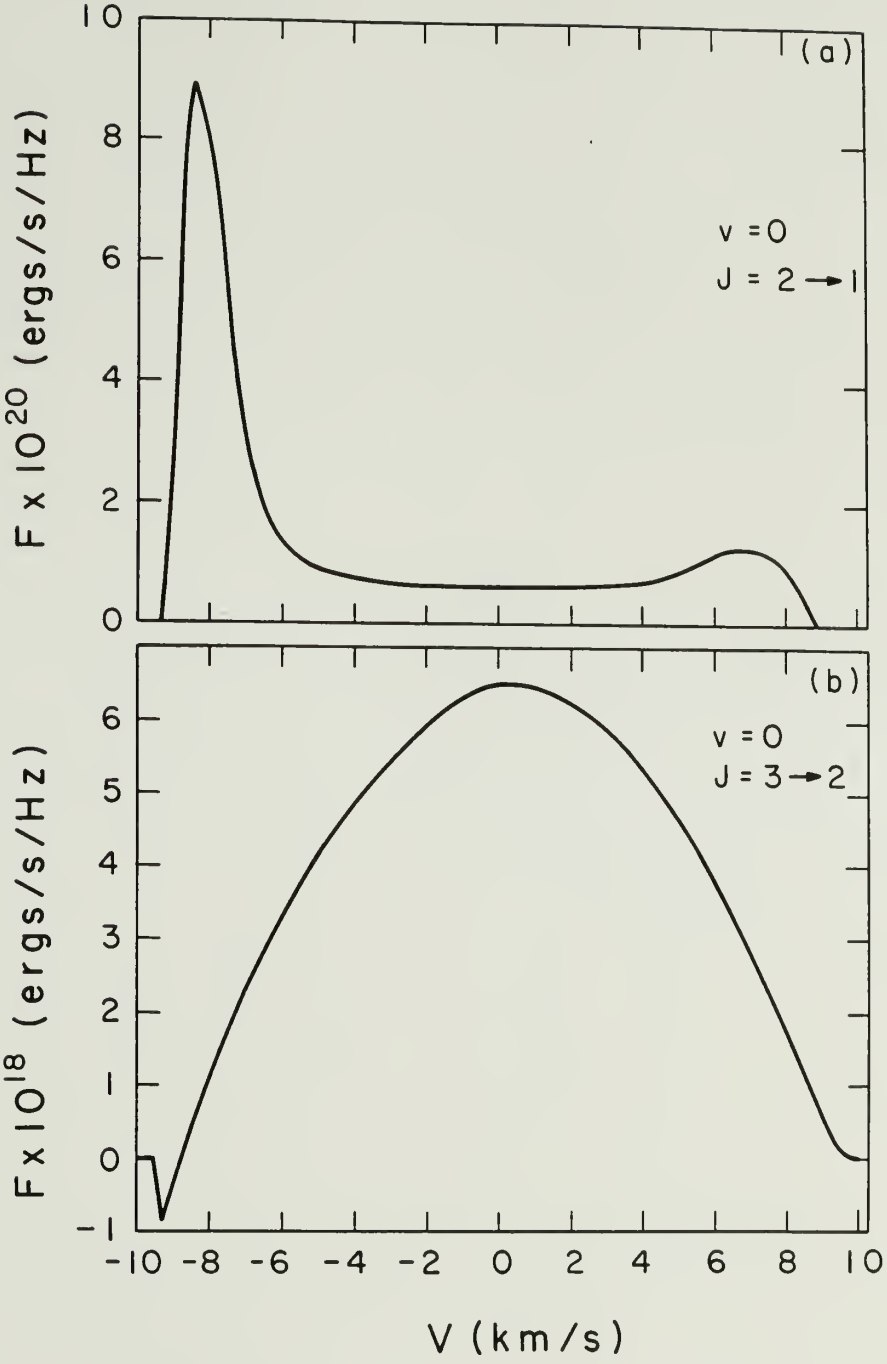
(a)
v = 0
J = 2 → 1
F x 10^20 (ergs/s/Hz)
(b)
v = 0
J = 3 → 2
F x 10^18 (ergs/s/Hz)
V (km/s)

shows the nonmaser $v = 0$, $J = 3 \rightarrow 2$ transition.

The results of small and large star calculations, with different rates of mass loss are presented in Table 1. In all cases, the terminal velocity and abundance of SiO are as given for the profiles in Figure 3. The numbers tabulated are the peak monochromatic luminosities, F, in $erg.s^{-1}.Hz^{-1}$. The designations m. and n.m. stand for maser and nonmaser transitions, respectively. An important point to notice is that $v = 1$ vibrationally excited maser transitions, which will be described in a later chapter, are antithetical to the presence of $v = 0$ ground state maser transitions, and vice versa.

Discussion

Variations of $\dot{M}$, v_∞, and f_{SiO} all change the number density of SiO molecules at any given radius. This causes the region where the optical depths of the $v = 1 \rightarrow 0$ lines are of order unity to move closer to, or farther from the stellar photosphere. Since the stellar continuum must be relatively strong in this region to produce ground state masers by anisotropic escape, those parameters effectively determine the character of the $v = 0$ rotational transitions. If the mass loss rate is high, the $v = 1 \rightarrow 0$ lines are very thick near the star, and the $v = 0$ populations do not invert; however, the KS radiative trapping process operates under these conditions, producing strong $v = 1$ masers (Kwan and Scoville, private communications).

TABLE 1

Peak Monochromatic Luminosities (ergs/s/Hz)

(a) Small Star

		$\dot{M}=1\times10^{-6}$ $M_\odot$/yr	$\dot{M}=2.5\times10^{-6}$ $M_\odot$/yr	$\dot{M}=5\times10^{-6}$ $M_\odot$/yr
v=0	J=1→0	3×10^{22} (m)	2×10^{22} (m)	8×10^{17} (nm)
	J=2→1	2×10^{22} (m)	9×10^{20} (m)	2×10^{18} (nm)
	J=3→2	1×10^{22} (m)	7×10^{18} (nm)	7×10^{18} (nm)
v=1	J=1→0	8×10^{17}	4×10^{17}	3×10^{19} (m)
	J=2→1	2×10^{18}	4×10^{17}	2×10^{21} (m)
	J=3→2	9×10^{17}	2×10^{18}	4×10^{21} (m)

(b) Large Star

		$\dot{M}=5\times10^{-6}$ $M_\odot$/yr	$\dot{M}=1.25\times10^{-5}$ $M_\odot$/yr
v=0	J=1→0	4×10^{22} (m)	6×10^{18} (nm)
	J=2→1	3×10^{21} (m)	2×10^{19} (nm)
	J=3→2	7×10^{18} (nm)	5×10^{19} (nm)
v=1	J=1→0	2×10^{18}	4×10^{20} (m)
	J=2→1	2×10^{18}	7×10^{21} (m)
	J=3→2	6×10^{18}	2×10^{22} (m)

Alternatively, when the mass loss rate is relatively low and if the $v = 1 \rightarrow 0$ lines have order unity optical depths near the star, $v = 0$ masers can be strong. Note that under these last conditions, the optical depths in the vibrational lines are never very high, a situation which makes radiative pumping of vibrationally excited masers impossible.

The luminosities of the stronger $v = 0$ masers in our model seem to be comparable to those observed for $v = 1$ masers associated with Mira variables. The photon fluxes for these tend to be on the order of 10^{43} to 10^{44} s^{-1} (Cahn and Elitzur 1979).

The relative intensities of the $v = 0$ rotational lines show interesting trends. Among the maser lines, the $J = 1 \rightarrow 0$ lines are always strongest, and the intensities fall with increasing J of the higher transitions. We have also seen that maser transitions may coexist with normal-appearing nonmaser lines, and that the maser lines are always the lower J transitions. Note that with a $v_\infty = 5$ km/sec large star model, there is only one strong maser line, the $v = 0$, $J = 1 \rightarrow 0$.

Summary

Let us recapitulate our conclusions:

1. Strong $v = 0$ SiO masers are made possible by the anisotropic

escape.

2. In sources which have strong $v = 0$ masers, the normally strong $v = 1$ masers will be weak or nonexistent.
3. In the $v = 0$ band, $J = 1 \rightarrow 0$ masers are always strongest.
4. Ground state maser lines in low J transitions may coexist with normal-appearing nonmaser emission in the same vibrational band.
5. Ground state masers occur when the number densities of SiO are lower than those in vibrationally excited SiO masers.

CHAPTER IV

EXCITED VIBRATIONAL STATE MASERS

Numerical Results

The numerical results for excited vibrational state masers are not quite as surprising as those for the $v = 0$ masers. Here we find that the DI anisotropic trapping and the KS radiative trapping processes operate pretty much as one would expect from the earlier work. We can, however, provide some new insight into the interplay of the velocity field and the various inversion mechanisms.

Table 2 shows peak monochromatic luminosities for vibrationally excited SiO in a number of models. All of these are maser lines, and in all cases the ground vibrational band has no inversions. We see from the table that inversions in the excited vibrational bands persist over a significant range of mass loss. The $v = 1$ masers are always the strongest, and of these the $J = 2 \rightarrow 1$ transition tends to dominate. The constancy of the luminosity of this particular transition is a consequence of the fact that it saturates before the other lines.

We have found that inversions in the excited vibrational bands are sustained throughout the inner envelope, and, hence for all values of ε, unlike the $v = 0$ inversions which exist only when $\varepsilon < 1$. Naturally, this causes the $v > 0$ masers to have slightly more complex

TABLE 2

Peak Monochromatic Luminosities (ergs/s/Hz)

Large Star

		5×10^{-6} $M_\odot$/yr	1×10^{-5}	1.25×10^{-5}
	1→0	1.7×10^{18}	7.4×10^{18}	4.1×10^{20}
v=1	2→1	1.6×10^{20}	7.2×10^{20}	6.7×10^{21}
	3→2	7.0×10^{20}	1.7×10^{21}	2.4×10^{22}
	1→0	3.8×10^{18}	2.7×10^{18}	3.3×10^{18}
v=2	2→1	1.5×10^{20}	1.2×10^{20}	1.0×10^{20}
	3→2	4.8×10^{19}	4.6×10^{19}	7.4×10^{19}
	1→0	4.0×10^{17}	4.7×10^{17}	5.6×10^{17}
v=3	2→1	1.5×10^{20}	1.2×10^{20}	1.2×10^{20}
	3→2	9.1×10^{19}	6.0×10^{19}	5.3×10^{19}

Small Star

		5×10^{-6} $M_\odot$/yr	1.5×10^{-6}
	1→0	2.9×10^{19}	4.0×10^{21}
v=1	2→1	1.5×10^{21}	1.1×10^{22}
	3→2	4.4×10^{21}	9.4×10^{21}
	1→0	7.8×10^{17}	1.3×10^{18}
v=2	2→1	2.3×10^{19}	6.4×10^{19}
	3→2	1.5×10^{19}	7.7×10^{19}
	1→0	2.4×10^{17}	3.1×10^{17}
v=3	2→1	3.3×10^{19}	2.0×10^{19}
	3→2	1.5×10^{19}	9.8×10^{18}

profiles than the ground state masers. These, typically in the $v = 2$ and $v = 3$ bands, have two components of varying strengths and widths. An example is shown in Figure 4. One component, usually quite broad, is centered on the stellar velocity. The other appears on the low velocity edge of the central component, and is the unocculted half of a front-back pair. The strongest lines show only one low velocity feature, resembling the typical $v = 0$ lines described in the previous chapter. Occasionally a "pedestal" of emission is present, but it is always much weaker than the spike components.

As with the $v = 0$ masers, all substantial inversions of the $v > 0$ rotational populations occur only within a few stellar radii of the center. The spatial extents of inversions of the various excited states overlap somewhat, but the regions of the most substantial inversions do not. Within each band, however, the dominant contributions to the maser lines come from the same part of the envelope. As one would expect, the higher the excitation of the transition, the closer to the star it is formed.

Velocity Profiles

The multiple components in the maser lines are a direct consequence of the assumed velocity law and the persistence of the $v > 0$ inversions. Since the maser intensities depend exponentially on the coherent path length along the line of sight, the maser lines are

Figure 4. The v = 2, J = 3 → 2 profile from the large star, $\dot{M} = 1 \times 10^{-5}$ $M_\odot$/yr model.

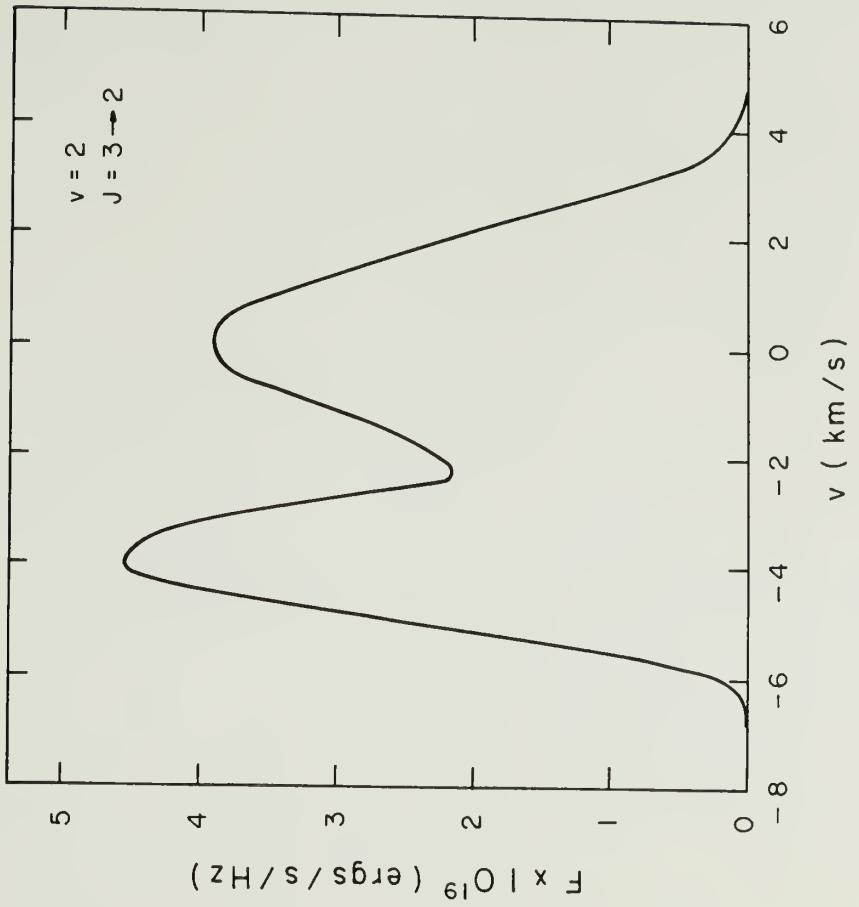
v = 2
J = 3→2
F x 10^19 (ergs/s/Hz)
v (km/s)
0
1
2
3
4
5
-8
-6
-4
-2
0
2
4
6

extremely sensitive to the velocity field. When ϵ is greater than one, as it is if the radius is less than 1.5 R_* for the assumed velocity law, the longest path lengths are perpendicular to the radial direction. Therefore, any maser emission from this region is centered on the stellar velocity, and has a width which reflects the outflow velocity at the radius of most substantial inversion. It is this situation which gives rise to the central component in many of our profiles.

The quantity ϵ is near unity when the radius is near 1.5 R_*, causing the optical path lengths to be almost isotropic. This can result in maser emission from this region mimicking the "thermal" lines of the $v = 0$ band. That is to say, they can be centered on the stellar velocity, quite broad, and roughly parabolic. This demonstrates that large line widths do not necessarily imply nonmaser emission. In fact, the only significant emission, of any width, from $v > 0$ bands that we have found is exclusively maser.

The blueshifted spike components arise in the envelope beyond 1.5 R_* where ϵ is less than one. In this part of the envelope, the longest optical paths are radial; hence, the velocities of the centers of these features give the outflow velocities at the radii of largest inversions. The widths of these features are always quite narrow, like the stereotypical maser feature. Because of the proximity of the masing region to the star, the red spike is always occulted by the stellar disk if ϵ is significantly less than unity. For these com-

ponents, the widths are indicative of the range of velocities, usually only 2 - 3 $km.s^{-1}$, in the masing region.

The fact that all of the strongest lines calculated are of the blue-spike variety has a very simple explanation. In the first place, it is physically impossible for a large portion of the envelope to have ε larger than one. Since

$$v(r) \alpha r^{\varepsilon} ,$$

ε characterizes the acceleration of the material. Since outflow velocities in Mira variables are known to be on the order of 10 $km.s^{-1}$ (e.g. Winnberg 1977), accelerations, and therefore ε, can be large only in small regions. This fact is reflected in our choice of velocity law. More importantly, rapid accelerations reduce the length of the coherent path. In the LVG approximation, the tangential optical depth is given

$$\tau_L(r) = \tau_o = \chi(r)/(V/r) , \text{ and} \qquad (1)$$

the radial optical depth is

$$\tau_*(r) = \tau_o/\varepsilon . \qquad (2)$$

We see that the tangential optical depth is, in a sense, fixed, while the radial optical depth may become arbitrarily large for small values of ε. This leads to the dominance of the blueshifted spikes in our results.

Inversion Mechanisms

We saw in the last chapter that the ground vibrational state masers exist only where ε is less than one. The contrasting ubiquity of the $v > 0$ masers is a consequence of the different kinds of pumping mechanisms effective for higher vibrational bands. We have confirmed that the DI anisotropic trapping process works well, and in fact dominates, in the inner parts of the envelope where ε is large. This is evidenced by the decline of the inversions, especially in the higher v bands, as ε decreases toward one. Of course, the DI mechanism, being complementary to the anisotropic escape process, does not operate where ε is less than or equal to one. The persistence of the $v > 0$ inversions is due entirely to the KS mechanism in our model.

The radiative trapping process operates much as Kwan and Scoville suggested, despite the more accurate radiative and collisional rates we have used. In fact, radiative pumping dominates, although collisional processes do make a contribution. To illustrate this, let us consider a typical region for $v = 1$ vibrational band masers. The hydrogen density is about 3×10^9 cm^{-3}, the kinetic temperature $\sim$ 1500K, and the excitation temperature $\sim$ 1000K. Einstein A coefficients for $\Delta v = 1$ and $\Delta v = 2$ transitions are typically 5 s^{-1} and 0.1 s^{-1}, respectively. Typical downward collisional rates for $\Delta v = 1$ and $\Delta v = 2$ are both about 2×10^{-14} $cm^3.s^{-1}$. The upward collisional rates for $\Delta v = 1$ and $\Delta v = 2$ are roughly 0.3 and 0.1 times the down-

ward rates, respectively.

As described in Chapter I, the KS mechanism operates when the rotational levels of the masing band are depopulated in proportion to the number of $\Delta v = 1$ lines to each, and populated in proportion to their degeneracy. The depopulation takes place via saturated 8μ lines which connect the band below. The indirect population may be either collisional or radiative. The collisional route is from the band directly below. A crude estimate of the collisional population rate for a typical level is

$$n\ (v = 0,\ J)\ .\ 10^{-15}\ cm^3.s^{-1}\ .\ 3 \times 10^9\ cm^{-3}\ ,$$

using values given above. Note that it is also the approximate rate at which collisions would populate the band above the masing band. Radiative population of the $v = 1$ band is from spontaneous decays from the band above, at a rate of

$$n\ (v = 2,\ J)\ .\ 5\ s^{-1}\ .$$

Considering the excitation temperature, we find that the radiative population rate is roughly 10^4 times that of the collisional process. Little question is left concerning the radiative dominance in our model.

One may argue that this result depends on the choices of collisional cross-sections, a choice we have made rather arbitrarily. In detail this is true, but not in general. Consider the argument

that we made in Chapter II that the rates at which inversions are pumped must exceed the pure rotational collisional rates in order to maintain any inversions. The pure rotational rates, whatever their actual values, must be orders of magnitude larger than the collisional vibrational rates. This fact alone can preclude any inversions if the radiative rates do not dominate the populations.

The peak inversions of each vibrational band's population always occur at different distances from the star. For example, the model in Table 2 with a mass loss rate of 1.25×10^{-5} $M_\odot$/yr has peak inversions in the v = 1, 2, and 3 vibrational bands at radii of 1.8 R_*, 1.3 R_*, and 1.1 R_*, respectively. Note that the velocity field causes maximum emission from the v = 1 masers to arise farther from the star than the region of peak inversion, a radius of 2.3 R_*. The most negative optical depths in the tangential direction (to facilitate comparison) are typically -6 to -8, and never more negative than -10. Regions of substantial inversion in different vibrational bands never overlap.

One may see why this happens in the context of the Kwan and Scoville mechanism. Since the radiative transitions dominate the collisions, the chief ways in and out of a vibrational band are the 8μ lines connecting it to the bands above and below. The rates of depopulation of the rotational levels in the band of interest are proportional to the number of lines out of each level, instead of to the degeneracy, when those lines are very optically thick. This inhibits depopulation of the higher J states, just as was required for

producing inversions. If the lines to the vibrational band above are also thick, however, there is no effective way to populate the levels in proportion to their degeneracy. The net result must be thermalization. Since only one SiO vibrational band, at a given number density, can have thin $\Delta v = 1$ lines to the band above, and thick to the band below, the inversions of different bands cannot be expected to overlap.

In the context of the DI mechanism, the impossibility of overlap in the inversions of different vibrational bands is even more obvious. For this mechanism to be effective, the 8μ lines from the masing band to the one below must be intermediate to thick or optically thin. This can be true for only one band at a given number density.

Maser Line Intensities

Inspection of the line strengths in Table 2 reveals a disturbing fact. The maser luminosities tend to be lower than those observed (cf. Cahn and Elitzur 1979). This fact is not unique to our model, but is shared by previous envelope calculations (e.g. Kwan and Scoville 1974). As noted earlier, the strongest transitions in the table are saturated, which means that it is very difficult to further increase the photon fluxes in these. If SiO masers are located in the circumstellar envelope, as we believe, then there must be some oversight or failing in our model which impairs the efficiency of the

inversion processes.

We need not look for a process to inhibit the efficiency of vibrationally excited SiO masers; we have already discussed one, anisotropic escape. We have already seen that the DI anisotropic trapping works in conjunction with the KS radiative trapping mechanism in the inner, high ε, regions of the envelope, so it should not be too surprising to find that the anisotropic escape process competes with the KS process in the large fraction of the envelope where the acceleration (and ε) is very low. We have already seen that the $v = 1$ masers can actually be turned off under some circumstances, but it is difficult to say how much the $v > 0$ maser efficiency is affected in general. To estimate the size of the effect, we have tried several models using a velocity law given by

$$v(r) = 3 \text{ km.s}^{-1} (r/R_*)^{1/2} . \qquad (3)$$

The constant value of $\varepsilon = 1/2$ is less favorable for the anisotopric escape process than the very small values afforded by our more realistic velocity law. Results for the small star calculations are given in Table 3.

The most obvious feature of these results is the significantly higher peak monochromatic luminosities in comparison to Table 2. Because of the relatively larger value of ε, these lines have widths of 2 - 3.5 km.s^{-1}, slightly broader than the blue components of Table 2. This implies that the photon fluxes of the maser lines in these

Table 3

Peak Monochromatic Luminosities (ergs/s/Hz)

Small Star $v \propto (r/R_*)^{1/2}$

$\dot{M}=2.5\times10^{-6}\ M_\odot/yr$

	v=0	v=1	v=2
J=1→0	7.6×10^{20} (m)	5.5×10^{21}	2.1×10^{21}
J=2→1	9.3×10^{19} (m)	8.7×10^{21}	9.7×10^{21}
J=3→2	7.3×10^{16} (nm)	4.7×10^{21}	1.1×10^{22}

$\dot{M}=5\times10^{-6}\ M_\odot/yr$

	v=0	v=1	v=2
J=1→0	4.1×10^{19} (m)	9.1×10^{21}	1.7×10^{22}
J=2→1	3.6×10^{18} (nm)	1.3×10^{22}	3.5×10^{22}
J=3→2	7.1×10^{18} (nm)	8.6×10^{22}	3.2×10^{22}

$\dot{M}=1\times10^{-5}\ M_\odot/yr$

	v=0	v=1	v=2
J=1→0	6.8×10^{17} (nm)	1.3×10^{22}	3.6×10^{22}
J=2→1	3.1×10^{18} (nm)	2.0×10^{22}	6.5×10^{22}
J=3→2	7.4×10^{18} (nm)	1.0×10^{22}	4.9×10^{22}

models are well within the observed range of 10^{43} - 10^{44} s^{-1} (Cahn and Elitzur 1979). The profiles of these lines are all of the simple negative velocity spike variety.

Presence of maser emission from the v = 0 band indicates that the value of $\varepsilon = 1/2$ does not entirely suppress the anisotropic escape process. Making ε closer to one may further increase the $v > 0$ pumping efficiency, but it also reduces the coherent path length in the radial direction. Maximum intensity in the maser lines would probably be obtained with a velocity law having a value of ε between 1/2 and 1. Unfortunately, there is not much justification for such a velocity law. As discussed earlier, one cannot expect steady accelerations through large portions of the envelope.

The relative intensities of the maser lines within each band show an interesting pattern in all the $v > 0$ models. The $J = 2 \rightarrow 1$ transition is always strongest, and the $J = 1 \rightarrow 0$ is always weakest. This is a necessary consequence of the radiative pumping and the SiO energy level structure. All levels, except the J = 0, have two 8μ lines to depopulate them downward. When masing occurs, they are populated in closer proportion to their degeneracy, 2J + 1. Therefore, where the ratio of the degeneracies of two adjacent levels is largest, one expects the largest inversions. This occurs for the lowest J values. Since only one line connects the J = 0 population to the next lower band, only half as many deexcitations are possible, in effect supporting the population. The $J = 1 \rightarrow 0$ populations are, therefore,

more difficult to invert. The net result is that the $J = 2 \rightarrow 1$ lines are always strongest. The same argument, with only slight modification, applies to the DI mechanism.

The dominance of the $J = 2 \rightarrow 1$ transition becomes less evident with increasing mass loss rate. This is caused by saturation, and is most obvious in the $\varepsilon = 1/2$ models of Table 3. When all the transitions saturate, the photon fluxes tend to be roughly the same. Observations suggest this is true in nature for $v = 1$ masers (Lane 1982, Clemens and Lane 1982).

Observations show that the $J = 2 \rightarrow 1$ line of the $v = 2$ band of SiO is anomalously weak by at least a factor of 50 (Olofsson et al. 1981). There is no indication of this in our numerical results. Deguchi (private communications) has suggested that the anomaly could be caused by a quirk in the collisional rates to one of the involved levels. The strong variations in the rates calculated by Bienick and Green (1982) lend some credence to this idea. It is impossible to prove this hypothesis since one cannot determine the actual collisional rates.

We have suggested another possible explanation for the weak $v = 2$, $J = 2 \rightarrow 1$ maser line. It was noted by Geballe and Townes (1974) that there is a near frequency coincidence between the RO line connecting the SiO $v = 2$, $J = 1$ level to the $v = 1$, $J = 0$ level, and $11_{6,6} \rightarrow 12_{7,5}$ transition of H_2O. At a frequency of 1219.15 cm^{-1}, these may well be within one Doppler width of each other (Camy-Peyret

and Flaud 1976). The consequence of this overlap is most likely a large increase in the opacity of that line, inhibiting the radiative deexcitation of the v = 2, J = 1 SiO level. Therefore, this level is probably maintained at a higher population than would otherwise be expected. This effect would increase the inversion of the J = 1 with respect to the J = 0 level, at the expense of the J = 2 → 1 transition.

We attempted to demonstrate the feasibility of the overlap hypothesis by modifying the statistical equilibrium equations to include the water line. Unfortunately, the resulting code proved to be so unstable that no useful results could be obtained.

Summary

Let us recapitulate our main conclusions concerning excited vibrational state masers:

1. We have confirmed that both the Kwan and Scoville, and the Deguchi and Iguchi mechanisms can produce inversions in the inner circumstellar envelope.
2. Multiple velocity components are possible using only a simple velocity law. Emission is always centered on the low velocity side of the stellar velocity.
3. The regions of substantial inversion of different vibrational

bands never overlap.

4. Line luminosities in the model are lower than those observed. Since the anisotropic escape process seriously reduces pumping efficiency, judicious choice of velocity law can boost the photon fluxes.

5. Our model cannot explain the anomalously weak $v = 2$, $J = 2 \rightarrow 1$ transition.

CHAPTER V

SEARCH FOR MASER EMISSION FROM THE v = 0, J = 1 → 0 TRANSITION OF SiO

Observations

The anistropic escape mechanism plays an important role in our numerical model. As we saw in the last chapter, it severly limits the pumping efficiency of excited vibrational state SiO masers. The more spectacular manifestations are, of course, the inversions of the v = 0 populations discussed in Chapter III, which give line luminosities comparable to those of the excited vibrational state masers. Since anisotropic escape seems to be solely responsible for ground state masers in our model, observations of such sources could indicate the basic validity of our calculations. Unfortunately, nature has not been too obliging on this point.

The few published searches for v = 0 SiO emission from stars have concentrated on the v = 0, J = 2 → 1 transition from sources with strong v = 1 masers. Of the fewer than 20 stars detected, only VY Canis Majoris (Buhl et al. 1975) and, possibly NML Cygni (Dickinson et al. 1978) show ground state maser emission. In both cases, the emission is much weaker than the excited vibrational state emission from the same sources. Both of these stars are supergiants, and as such our results may not be applicable to them, since we have modeled giant stars.

As a more definitive test of our model predictions, we decided to choose more likely candidate stars and search for ground state masers ourselves. According to our results, $v = 0$ masers should be found in sources that are identical to the excited vibrational state SiO maser stars, except for a somewhat lower mass loss rates. Only a few percent of all Mira variables, and a smaller fraction of semiregular variables, show maser emission. If one assumes that differences in mass loss rates are partially responsible for the presence or absence of the $v > 0$ masers, then one would expect that some of the undetected Mira and semiregular variables would show ground state masers. We, therefore, chose our sources from lists of nearby giants of these types. Following the example of excited vibrational state masers, we thought that only a small fraction of the source list would be likely to show ground state emission, so we elected to search a large number of stars.

Since the $v = 0$, $J = 1 \rightarrow 0$ transition is most likely to mase, we chose to search at the corresponding frequency of 43.423798 GHz. The search was carried out at Haystack, using the 1024 autocorrelator, and at FCRAO, using the 256 x 1/4 MHz filters, in the spring of 1981. No maser emission was detected. A list of sources and antenna temperature upper limits is given in Table 4. Table 5 presents the upper limits on monochromatic luminosities (F). The source type, Mira (M) or semiregular variable (SR), distance, and published detections (+) or non-detections (-) in other molecules are also presented.

TABLE 4

Source List

	Source	α_{1950}	δ_{1950}	V_{LSR}	$T_A^* <$
1.	And VX	$0^h17^m15.^s0$	44°25'56"	-10 km.s^{-1}	0.2K
2.	And R	0 21 23.0	38 18 02	-10	0.25
3.	And EF	0 36 58.3	46 16 52	-9	0.25
4.	Per U	1 56 14.8	54 34 49	-11	0.4
5.	And UX	2 30 13.1	45 26 06	-6	0.3
6.	Tri R	2 34 00.0	34 02 48	-3	0.25
7.	Cas CQ	2 42 40.0	62 47 48	-8	0.25
8.	Ari T	2 45 32.0	17 18 07	2	0.2
9.	Cam T	4 35 13.0	66 02 54	-9	0.25
10.	Ori W	5 02 48.6	01 06 37	11	0.2
11.	Aur S	5 23 49.0	34 06 24	3	0.25
12.	Aur U	5 38 55.0	32 01 06	4	0.25
13.	Aur UU	6 33 06.6	38 29 16	2	0.25
14.	Lyn U	6 36 18.0	59 57 24	-17	0.3
15.	Gem R	7 04 20.8	22 46 57	7	0.25
16.	C Mi S	7 30 00.2	8 25 35	12	0.25
17.	Cnc T	8 53 48.9	20 02 30	5	0.25
18.	U Ma R	10 41 07.9	69 02 19	-11	0.4
19.	U Ma RY	12 18 04.0	61 35 13	-11	0.25
20.	C Vn U	12 44 57.0	38 38 24	-31	0.2
21.	Boo V	14 27 44.2	39 04 59	-14	0.2
22.	Boo RW	14 39 06.2	31 47 07	-14	0.25
23.	Cr B V	15 47 44.1	39 43 23	-16	0.2
24.	Ser R	15 48 23.2	15 17 03	24	0.25
25.	Cr B RS	15 56 39.1	36 09 49	-17	0.25
26.	Her S	16 49 37.1	15 01 28	-15	0.2
27.	Her 01	17 12 21.9	14 26 45	-17	0.25
28.	IRc10381	17 48 28.0	-8 00 42	-15	0.3
29.	Lyr V	19 07 07.0	29 34 42	-11	0.2
30.	Cyg CH	19 23 14.2	50 08 31	-18	0.25
31.	Dra UX	19 23 22.4	76 27 42	-15	0.35
32.	Cyg R	19 35 28.7	50 05 12	-17	0.3
33.	Cyg FF	20 36 59.0	37 42 36	-16	0.25
34.	Cyg V	20 39 41.3	47 57 45	10	0.2
35.	Cyg DR	20 41 46.0	37 58 24	-16	0.3
36.	Cyg AB	21 34 24.5	31 52 39	-15	0.3
37.	Cep 12	21 41 58.5	58 33 01	-15	0.3
38.	Cyg WY	21 46 43.0	44 01 00	-15	0.3
39.	Peg TW	22 01 41.0	28 06 30	-19	0.25
40.	Peg RV	22 23 20.0	30 13 06	-26	0.3
41.	Cep W	22 34 32.7	58 10 00	-15	0.3

TABLE 5

Source Properties

Source	Type	Distance	OH, H_2, SiO (v>0)	F>
1. And VX	SRa	282 pc		$2x10^{21}$ergs/s/Hz
2. And M	M	308		$2x10^{21}$
3. And EF	SRa	104		$3x10^{20}$
4. Per U	M	510		$1x10^{22}$
5. And UX	SRb	289		$2x10^{21}$
6. Tri R	M	332		$3x10^{21}$
7. Cas CQ	SRb	247		$2x10^{21}$
8. Ari T	SRa	254		$1x10^{21}$
9. Cam T	M	484		$6x10^{21}$
10. Ori W	SRb	271		$1x10^{21}$
11. Aur S	SRa	263		$2x10^{21}$
12. Aur U	M	527	- +	$7x10^{21}$
13. Aur UU	SRb	244		$1x10^{21}$
14. Lyn U	M	1079	+ +	$3x10^{22}$
15. Gem R	M	338		$3x10^{21}$
16. CMi S	M	509		$6x10^{21}$
17. Cnc T	SRa	223		$1x10^{21}$
18. UMa R	M	497		$1x10^{22}$
19. UMa RY	SRa	201		$1x10^{21}$
20. CVn U	M	701	+ + -	$1x10^{22}$
21. Boo V	SRa	277		$2x10^{21}$
22. Boo RW	SRb	246		$2x10^{21}$
23. CrB V	M	571		$6x10^{21}$
24. Ser R	M	308	- + -	$2x10^{21}$
25. Cr B RS	SRa	262		$2x10^{21}$
26. Her S	M	487		$5x10^{21}$
27. Her 01	SRc	177		$8x10^{20}$
28. IRc10381	-	-	+ - -	-
29. Lyr V	M	579	+ - -	$7x10^{21}$
30. Cyg CH	SRa	255		$2x10^{21}$
31. Dra UX	SRb	287		$3x10^{21}$
32. Cyg R	M	344		$4x10^{21}$
33. Cyg FF	M	546		$7x10^{21}$
34. Cyg V	M	454		$4x10^{21}$
35. Cyg DR	M	468		$7x10^{21}$
36. Cyg AB	SRb	259		$2x10^{21}$
37. Cep 12	SRc	94		$3x10^{20}$
38. Cyg WY	M	496		$7x10^{21}$
39. Peg TW	SR	133	+ + -	$4x10^{20}$
40. Peg RV	M	1414		$6x10^{22}$
41. Cep W	SRc	323		$3x10^{21}$

Discussion

Perhaps interesting in some other context, lower, more precise values in Table 4 would not be more important here than the fact that there are no 10K maser lines from the v = 0, J = 1 → 0 SiO transition in any of these sources. This leaves us with the question of why our model predicts these masers, and yet nature does not produce them. Obviously these results are telling us something about maser stars, but we are not understanding the message.

We feel that our choice of velocity law is very reasonable, but it is by no means the only possibility. Considering that we know the inversion mechanisms, especially anisotropic escape, are very sensitive to the velocity field, perhaps we should reconsider our choice. To completely suppress the v = 0 masers at all mass loss rates, the value of ε cannot be much less than unity over large portions of the envelope. Since a large value of ε implies a large acceleration, it is difficult to imagine this is a viable solution. After all, SiO emission covers a relatively small velocity range in most maser stars. In addition, maser lines tend to be quite narrow, indicating little acceleration across the maser region. Finally, calculations of the type of velocity law expected for a radiatively driven flow (e.g. Kwok 1975) always produce a rapid acceleration in a very thin region with much larger regions of little or no acceleration.

Another suggestion is that the SiO may, under some conditions,

condense on dust grains, leaving so little SiO in gas phase that no masers may exist in any vibrational band. The efficiency of the dust in removing SiO from the envelope may be quite high, and in fact has been estimated to be as high as 99% by Morris and Alcock (1977). However, this still leaves sufficient SiO to produce "thermal" ground state lines at distances of at least 100 stellar radii from the star. The presence of $v > 0$ masers indicates a large amount of gaseous SiO close to the star. One would think that there would also be gas phase SiO between these two extremes.

The temperature of the envelope near the stellar photosphere is much too high to allow the survival, let alone formation, of dust grains. Some calculations simply assume that the dust evaporates at the rather high temperature of 1800K (Taam and Schwartz 1976, Schwartz 1975), leading to an inner radius of 2 or 3 stellar radii for the dust shell. A less arbitrary calculation by Deguchi (1980) finds an inner shell radius of 4 to 6 stellar radii. These estimates place almost all of our model's maser region within the cavity of the dust shell, where grain formation can have no effect on the SiO number density. We, therefore, feel that dust formation alone cannot account for the failure to observe ground state masers.

In the last two chapters, we saw that the high mass loss rates that favor $v > 0$ masers produce no ground state masers. One might speculate that whatever mechanism drives the mass loss also requires a lower limit on the SiO number densities in the inner envelope, and

so precludes ground state masers. In our time-independent, spherically symmetric model, this would mean a prohibitively high limit on the mass loss rate, 10^{-5} $M_{\odot}$/yr or more, when estimates from optical observations are one or two orders of magnitude lower. In reality nonuniformity in the mass loss may well lessen the severity of the constraint.

Another possibility is that the LVG approximation may break down for very low values of ϵ and lead to erroneous profiles in our model. In the outer part of the maser region, between five and ten stellar radii, very low accelerations lead to very long path lengths and large maser amplifications, if there are inversions. It also means that "thermal" material farther out in the envelope may lie within one Doppler width of the outer masing material. In a real envelope, some of the maser emission would be absorbed in the envelope itself, rather than contributing to the line luminosity, a fact not recognized in the LVG approximation. Of course, this can only apply to emission originating quite far out in the maser region, and, therefore, cannot be a complete solution to our ground state maser problem.

Recall that it is the anisotropy of the 8μ radiation from the star which drives the ground state masers. We have however ignored another source of pumping radiation, the circumstellar dust shell, which must affect the isotropy. In the next chapter, we investigate this factor.

CHAPTER VI

RADIATIVE PUMPING OF SiO MASERS BY DUST SHELLS

VY Canis Majoris

Deguchi et al. (1982) have searched for the v = 0, J = 2 → 1 transition of ^{28}SiO, ^{29}SiO, and ^{30}SiO in a number of sources, and have detected both ^{28}SiO and the less abundant ^{29}SiO in Orion, IRC 10216, and VY CMa. The VY CMa spectra are of particular interest to us, since they may provide some insight into the ground state maser mechanism and the physical conditions in the maser region.

The profile of the ^{28}SiO emission, which originates with the most abundant silicon monoxide species, differs very little from that of Buhl et al. (1975). There are essentially two components to the line, one very broad and weak, and a second narrow and stronger, both of which are centered on the stellar velocity (~ 18 $km.s^{-1}$). The broad feature is roughly parabolic, of peak temperature ~ 0.2K, and is considered to be the familiar "thermal" emission. Its full width, probably indicating the outflow velocity of the envelope, is about 60 $km.s^{-1}$. The spike feature has peak temperature ~ 0.8K and a full width of roughly 10 $km.s^{-1}$. Until Deguchi et al. detected ^{29}SiO in VY CMa, the spike component was the only ground state SiO maser emission unambiguously associated with a late-type star.

The ^{29}SiO profile is very different from that of the ^{28}SiO.

Deguchi et al. describe three separate components in it:

1. Broad weak emission:

   This is centered on the stellar velocity, and has a full width of ~ 40 $km.s^{-1}$. Because of the low antenna temperature (~ 0.1K), the shape is indeterminate.

2. Main feature:

   This is also centered on the stellar velocity. It is quite strong, ~ 1.7K. Its width is about 15 $km.s^{-1}$, and its shape is roughly parabolic.

3. Spike features:

   Surmounting the main feature are four narrow (~ 3$km.s^{-1}$) spikes with antenna temperatures between 0.1K and 0.4K. These are almost symmetric about the stellar velocity.

We can make some reasonable arguments for the maser nature of the spike component of the ^{28}SiO profile. Perhaps most compelling is the fact that it is much stronger than the "thermal" component, suggesting a nonthermal origin. In addition, it is not as narrow as some maser spikes, but it is still very much narrower than the velocity extent of both the nonmaser ground state emission and the excited vibrational state maser emission from this source. Finally, its shape is not at all reminiscent of the parabolic or rectangular profiles which usually characterize nonmaser molecular envelope emission.

We can apply the same arguments to the ^{29}SiO line to suggest a nonthermal origin. Those are especially compelling for the spike

features. Comparison of the line intensity to that of the ^{28}SiO should remove any remaining doubts about the maser origin of the emission. Although the abundance ratio of ^{28}Si to ^{29}Si is expected to be about 20, the temperature of the ^{29}SiO lines is at least twice that of the ^{28}SiO.

VY CMa is a supergiant star, and is, therefore, somewhat different than the Mira variables we have tried to model to this point. It is thought to have an effective temperature of 2700K, a mass loss rate of 10^{-4} $M_{\odot}$/yr, and a radius of 1.8×10^{14} cm or 2.5×10^{14} cm (Taam and Schwartz 1976, Apruzese 1975). The chief difference seems to be one of scale, so qualitive information concerning this star should apply to Miras as well. In Chapter IV, we saw that the velocity law influences the maser line profiles in several ways. If we apply those ideas to the data of Deguchi et al. we may be able to learn something that will allow us to improve our envelope model.

We know that envelope emission centered on the stellar velocity, as both the ^{28}SiO and ^{29}SiO ground state masers are, comes from optical paths that are perpendicular to the radial direction. This can only occur for maser emission when these are the longest paths, which requires that ε (d ln V/d ln r) be greater than one. This in turn requires large accelerations in the maser region. A reassuring point is that the large ε is consistent with the broad line widths, in comparison to other maser profiles of these features. The widths then should represent the outflow velocities in the two maser regions.

Since the ^{29}SiO maser emission is broader, it must originate in a higher velocity region, which would be farther from the star for a monotonically increasing velocity law.

The small spikes on the ^{29}SiO population look tantilizingly like the front-back pairs that were discussed in earlier chapters. Since there are two pairs, and they overlap the broader emission, these cannot be interpreted in terms of a simple time-independent velocity law. They are also minor in comparison to the main feature, so for the time being we will avoid unnecessary complications by ignoring these features.

A comparison of our ground state maser model to the VY CMa observations is rather discouraging, since the main points are almost completely different. For example, profiles in our models are always narrow with a single blue component in contrast to Deguchi's spectra. More fundamentally, the radiative pumping requires that the less abundant isotope mase in a region of higher density, which must be closer to the star. For an expanding envelope, that also requires that the outflow velocity be less, once again contradicting the observations.

Perhaps our model is just too simple to interpret these details. After all, VY CMa is a very complex object. The peaks of both ^{28}SiO and ^{29}SiO profiles at the stellar velocity is, however, quite unambiguous. The implication of $\varepsilon > 1$ is crucial to the pumping mechanism itself, since the anisotropic escape process works best when

$\varepsilon \ll 1$, and not at all when $\varepsilon > 1$. With no viable alternative ground state maser mechanism, we are left with serious questions concerning the completeness of the numerical model.

Using stellar parameters for VY CMa, we have attempted to produce something from our model resembling the observations. We succeeded in producing ground state maser emission from the ^{28}SiO and ^{29}SiO, but, unfortunately, it conforms exactly to the same rules determined for the Mira models. We tried to produce stellar velocity peaks in the line profiles by forcing the velocity law to favor inversions at higher values of ε, but no inversions could be produced in the $v = 0$ band when $\varepsilon \geq 1$. No significant maser emission was generated at zero velocity. Clearly, our model fails to account for some basic property or attribute of the supergiant maser region.

Although the ground state inversion mechanism they describe is actually that of Kwan and Scoville (1974), rather than the anisotropic escape process, Deguchi et al. have also recognized the inability of our simple models to reproduce the observed profiles. They hypothesize that a rotating disk-shaped envelope, rather than a spherical geometry, might be able to explain the data. Inversions would be produced by the anisotropic escape process, but the optical path lengths and velocity structure would be changed by the geometry. Longest coherent paths would still be radial, but these would yield emission peaks at zero velocity, since the motion of the material is perpendicular to the line of sight. Presumably, inner parts of the

disk would rotate more rapidly than the outer, explaining the broader width of the ^{29}SiO profile, since it is formed closer to the star than the ^{28}SiO.

The numerical model for a spherically symmetric envelope is already quite complicated, and requires a healthy amount of computer time to produce line profiles. The introduction of a disk geometry to the code would necessitate additional numerical integrations over angle for a full range of disk orientations, increasing the calculation time, perhaps prohibitively. Before resorting to the disk, we have chosen to investigate an alternative which retains the spherical geometry while still offering some hope of solving the problems we have discussed.

We have already noted that, because of the temperature contraints, most of the SiO maser region must lie within the cavity of the circumstellar dust shell. Since most of the optical radiation of the star is absorbed by the dust shell, and subsequently reradiated in the infrared, one may expect the dust to have some effect on the radiative pumping of the SiO. Intuitively, one would expect the inclusion of the dust to raise the general level of excitation of the SiO, and to raise the maser luminosities, by contributing additional infrared pumping photons.

For both the anisotropic trapping and anisotropic escape processes, it is the angular distribution of 8μ photons, not simply their quantity, which drives the population inversions. One might expect

the dust shell to contribute to the isotropy of the infrared, since it completely surrounds the maser region, whereas the star subtends only a small solid angle. The 8μ flux from the dust, however, is not itself isotropic in the maser cavity because of the optical thinness and geometry of the shell. In fact, the strongest infrared flux from the shell lies along the directions perpendicular to the radius from an envelope point to the star.

For the purposes of illustration, let us ignore the star for the moment, and consider a uniform dust shell of finite spatial thickness. Figure 5 represents the cross-section of such an object. The parameters are as follows:

R_o = outer shell radius

R_i = inner shell radius

r = distance from center

$\mu = \cos \theta$.

The path length through the shell along a line originating at a radius r and in a direction θ is then

$$\ell(r, \mu) = [R_o^2 - r^2 (1 - \mu^2)]^{1/2} - [R_i^2 - r^2 (1 - \mu^2)]^{1/2} . \quad (1)$$

The path length is a minimum for the radial directions, $\mu = \pm 1$, and a maximum for the tangential directions, $\mu = 0$. For the case of a

Figure 5. Schematic diagram of finite, uniform dust shell.

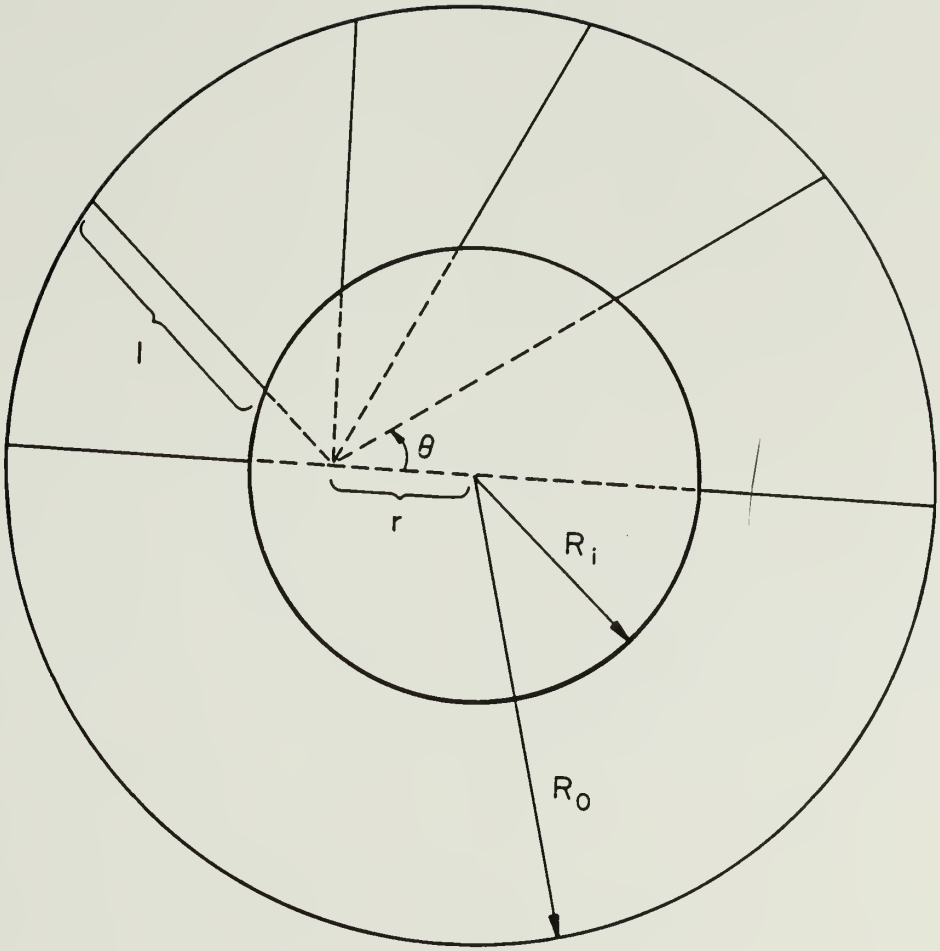
l
θ
r
R_i
R_o

uniform, optically thin shell, the intensity of the infrared is proportional to the path length multiplied by the dust's emission coefficient; therefore, there are more 8μ pumping photons along the tangential direction, perpendicular to the direction of pumping photons from the star. The anisotropy of the dust infrared is non-existent at the exact center, and grows to a maximum as the radial distance approaches the inner edge of the shell.

Still ignoring the star, we may ask what this means for the important maser mechanisms. Let us repeat the illustration given in Chapter III, substituting the escape probability in the tangential direction, β_L, for β_*. As before, the optically thin case ($\tau_o << 1$) gives the limiting ratio

$$\beta_L/\bar{\beta} = 1 .$$

For the optically thick case ($\tau_o >> 1$),

$$\beta\ (r, \mu) \to [1 + \mu^2\ (\varepsilon - 1)]/\tau_o\ (r) , \text{ and}$$

$$\beta_L\ (r) \to 1/\tau_o\ (r) .$$

As before,

$$\bar{\beta}\ (r) \to [1 + (\varepsilon - 1)/3]/\tau_o\ (r) .$$

Therefore,

$$\beta_L/\bar{\beta} = 3/(2 + \varepsilon) \qquad (\tau_o >> 1) \tag{2}$$

(cf. Equation (3) of Deguchi and Iguchi 1976, Equation (6) of Chapter III). Similarly, one could construct a figure resembling Figure 1, showing lines of constant ε on a plot of $\beta_L/\bar{\beta}$ vs. τ_o.

Since the high and low optical depth limits for $\beta_L/\bar{\beta}$ are not the same, and τ_o is different for each line, we once again have a situation where the anisotropy of the radiation and the velocity fields may produce inverted populations. In comparison to the anisotropic escape and DI ansisotropic trapping mechanisms, however, the acceleration regimes (as characterized by ε) are reversed. Consider the case of large ε and the $v = 0$ band. With $\varepsilon > 1$, $\beta_L/\bar{\beta}$ becomes smaller with increasing opacity, and the opacities of the $v = 1 \rightarrow 0$ lines increase with the J values of the rotational levels. Therefore the lower J levels are more likely to absorb a dust photon in relation to the likelihood of reradiating the same photon than the higher J levels are. This is exactly the same effect we discussed for the anisotropic escape process in the case of $\varepsilon < 1$. We might then expect this to produce ground state masers in regions of high ε, and, therefore centered at the stellar velocity, if there were no 8μ flux from the star.

Similarly, the ansisotropic trapping process might take place in low ε regions, if only the dust contributed pumping photons. If $\varepsilon < 1$, $\beta_L/\bar{\beta}$ is greater for increasing opacity, and, therefore, increasing J. That implies that the dust photons are more likely to promote an SiO molecule to a higher J level than one of lower J. The

result being that the lower v bands selectively lose more of the high J populations, and inversions of the excited vibrational state populations could result.

Both star and dust shell are present in reality, and both must affect the SiO maser mechanisms. Observations of Mira variables show that the 8μ flux is dominated by dust emission (e.g. Sherwood et al. 1977, Merrill 1977), but very close to the stellar photosphere the dust infrared is only a small fraction of the radiation field. At the distance of the SiO maser region, it is not immediately obvious that either dust or stellar 8μ photons dominate, and one can imagine a situation in which the maser region is subdivided by a change in the radiation's anisotropy. In the inner region, everything would take place much as it does in our models without dust, but in the outer layers, the pumping mechanisms would be reversed in ε by the dust infrared. Such a scenario could lead to very complex line profiles, caused by the mutliple inversion methods and regions, from even simple physical parameters.

Numerical Dust Shell Model

We have chosen to investigate the effects of spherical dust shells on SiO masers by using the simplest possible physical model. The shell is assumed to start at a distance R_i from the center and extend to infinity. The opacity of the dust is

$$\kappa\,(r) = 0 \quad \text{for} \quad r < R_i \ , \ \text{and}$$
$$\kappa\,(r) = \kappa_o\,(r/R_*)^{-2} \quad \text{for} \quad r \geq R_i \ . \tag{3}$$

This would exactly describe a situation in which all dust instantaneously forms at R_i, and then flows outward with constant velocity. In reality, the dust must form over a range of radius, but this is cancelled to some extent by the acceleration which takes place simultaneously.

The optical depth in the dust along some path, ℓ, is then

$$\tau\,(\ell) = \int_0^1 d\ell\ \kappa(\ell) \ . \tag{4}$$

For a path originating at a radius r_p and extending to a radius r,

$$\ell\,(r_p, \mu) = r_p\,\mu \pm [r^2 - r_p^2\,(1 - \mu^2)]^{1/2} \ . \tag{5}$$

The plus or minus is chosen opposite to that of the direction cosine, μ. The optical depth can be integrated analytically to give

$$\tau\,(\ell) = (\kappa_o\,R_*^2/p)\,\tan^{-1}\,[(\ell - r_p\,\mu)/p] - \tau_o \ , \quad \text{where}$$
$$p = r_p\,(1 - \mu)^{1/2} \ . \tag{6}$$

For the case in which the optical path is entirely within the dust (i.e. it does not cross the cavity),

$$\tau_o = (\kappa_o\,R_*^2/p)\,\tan^{-1}\,(-r_p\,\mu/p) \ . \tag{7}$$

If the path originates within the shell cavity (i.e. $r_p < R_i$),

$$\tau_o = (\kappa_o R_*^2/p) \tan^{-1} [(R_i^2 - p^2)^{1/2}/p] . \quad (8)$$

Finally, if the path originates in the dust and crosses the cavity,

$$\tau_o = (\kappa_o R_*^2/p)[\tan^{-1} (-r_p \mu/p) + 2 \tan^{-1} [(R_i^2 - p^2)^{1/2}/p]] . \quad (9)$$

Taam and Schwartz (1976) have computed dust temperatures as a function of radius for a number of dust density power law distributions in the course of modeling dust shells around late-type giants. Their results do not differ markedly from the $r^{-1/2}$ law that we earlier assumed for the gas kinetic temperature. We, therefore, assume the dust temperature is given by

$$T_d (r) = T_* (r/R_*)^{-1/2} . \quad (10)$$

Following Andriesse and Olthof (1973), and Schwartz (1975), we also assume that the dust grains are large enough so that they radiate like black bodies at wavelengths shorter than 30μ.

The continuum energy density contributed by the dust shell along any path then becomes

$$I_d (r_p, \mu) = \int_0^{\tau_{max}} d\tau \, B_d (\tau) \exp (-\tau) . \quad (11)$$

$B_d (\tau)$ is the Planck function for the dust temperature at the point defined by the optical depth, τ, and

$$\tau_{max} = \tau (\ell = \infty) = (\pi \kappa_o R_*^2/2p) - \tau_o (r_p, \mu) . \quad (12)$$

Fortunately for us, the dust shells around Mira variables and VY CMa, are thought to be optically thin at a wavelength of 8μ. This means that even on a global scale the effect of the dust on the radiative transfer in the optically thick $\Delta v = 1$ lines is of secondary importance. The primary assumption of the LVG approximation, that we have used, is that the velocity gradients decouple small regions of the envelope, and, therefore, reduce the line transfer to a completely local problem. On a local scale, the dust can have even less effect; thus, we can ignore what local dust is mixed with the gas. We can adequately treat the effects of the dust shell by considering only its contribution to the ambient continuum radiation, and ignoring its small local continuum opacity.

In Chapter II, we stated that the radiation field was given by Equation (II.18),

$$J(r) = (1 - \bar{\beta})\, S(r) + I_* \beta_c$$

Considering the dust shell, the continuum term must now consist of a term for both star and dust shell. The radiation field becomes

$$J(r) = (1 - \bar{\beta})\, S(r) + 1/2 \int_{-1}^{\mu_c} d\mu\, I_d(r, \mu)\, \beta(r, \mu) + 1/2 \int_{\mu_c}^{1} d\mu\, I_s(r, \mu)\, \beta(r, \mu) . \tag{13}$$

I_s is the contribution from both star and dust in the direction of the stellar disk.

$$I_s(r, \mu) = I_d(r, \mu) + I_* \exp(-\tau_*) \quad \text{for} \quad \mu > \mu_c \,. \tag{14}$$

τ_* is the optical depth in the dust from the radial point at r to the edge of the dust shell cavity.

To be more consistent with the dust shell parameters, we changed the velocity law for the gas outflow. Inside the cavity, we assume a slowly accelerating flow:

$$v(r) = v_o (r/R_o)^{1/2} \,. \tag{15}$$

This joins smoothly to a law more appropriate for a radiatively driven flow inside the dust shell,

$$v(r) = v_\infty (1 - R_o/r)^{1/2} \,. \tag{16}$$

Presumably, this mimics the behavior of a real envelope, which would undergo rapid acceleration only after dust grains form, and radiation pressure may act on them. Because grains do not grow instantaneously, we assume that the radiation pressure becomes important a little sooner than the dust's infrared emission. We, therefore, take R_o to be 0.4 R_* smaller than the inner edge of the shell, R_i. The two separate velocity expressions then join at 1.1 R_o, so

$$v_o = 0.29 \cdot v_\infty \,. \tag{17}$$

To set κ_o for each set of vibrational lines, we have assumed that the optical depths in the radial direction must be equal to those suggested by Apruzese (1975). That is to say,

$$\kappa_o (\Delta v) = \tau_{max} (\mu = -1, \Delta v) \cdot R_i/R_*^2 \cdot \quad (18)$$

Following Deguchi (1980), we take $R_i = 4R_*$ for the Mira model. For VY CMa, we take $R_i = 2.5\ R_*$ to be consistent with Taam and Schwartz (1975). In both cases, f_{SiO} is assumed to be constant throughout the envelope. Finally, the additional computing time required by integrations through the dust shell necessitated a decrease in the number of vibrational bands included to 3.

A summary of physical parameters for Mira and VY CMa models appears in Table 6.

Numerical Results

The results from the new and improved model are different from the earlier ones in a number of ways. In order to separate the effects of the new velocity law from those of the dust shell, we have run two models for each mass loss rate, one with dust and one without. Peak monochromatic luminosities and the velocities of those peaks are given for the Mira models in Table 7. Table 8 presents the same information for the VY CMa model with the nominal mass loss rate of $1 \times 10^{-4}\ M_\odot$/yr. As before, the v = 0 lines are designated (m) and (nm) for maser and nonmaser emission, respectively. There are no luminosities for the ground state of the $10^{-5}\ M_\odot$/yr Mira model with dust because of a convergence failure.

TABLE 6

Summary of Model Parameters

	Mira	VY CMa
R_*	3×10^{13} cm	2.54×10^{14} cm
T_*	2700 K	2700 K
R_i	4 R_*	2.5 R_*
v_∞	20 km.s^{-1}	35 km.s^{-1}
τ_{max} (μ = -1, Δv = 1)	0.25	0.07
τ_{max} (μ = -1, Δv = 2)	1.2	0.2
τ_{max} (μ = -1, Δv = 3)	3.2	0.6
f_{SiO}	3×10^{-5}	3×10^{-5}

TABLE 7

Mira Model: Peak Monochromatic Luminosities, Velocity of Peak (ergs/s/Hz, km/s)

Without Dust

		$\dot{M}=1\times10^{-6}$ $M_\odot$/yr	$\dot{M}=5\times10^{-6}$ $M_\odot$/yr	$\dot{M}=1\times10^{-5}$ $M_\odot$/yr
v=0	J=1→0	9.2×10^{21}, -4 (m)	7.3×10^{21}, -16 (m)	4.2×10^{21}, -16 (m)
	J=2→1	4.5×10^{21}, -4 (m)	1.2×10^{21}, -16 (m)	1.7×10^{20}, -15 (m)
	J=3→2	2.8×10^{20}, -4 (m)	5.4×10^{19}, 0 (nm)	1.1×10^{19}, 0 (nm)
v=1	J=1→0	1.8×10^{16}, 0	3.6×10^{22}, -4	3.9×10^{22}, -5
	J=2→1	1.5×10^{17}, 0	4.2×10^{22}, -4	5.9×10^{22}, -5
	J=3→2	7.9×10^{17}, 0	2.1×10^{22}, -4	2.8×10^{22}, -5

Dust Included

v=0	J=1→0	6.5×10^{21}, -4 (m)	8.8×10^{21}, -16 (m)	-
	J=2→1	2.8×10^{21}, -4 (m)	1.5×10^{21}, -16 (m)	-
	J=3→2	2.7×10^{19}, 0 (nm)	2.9×10^{19}, 0 (nm)	-
v=1	J=1→0	4.1×10^{16}, 0	3.1×10^{22}, -4	6.2×10^{22}, -5
	J=2→1	5.2×10^{17}, 0	4.6×10^{22}, -4	8.3×10^{22}, -5
	J=3→2	2.4×10^{18}, 0	2.2×10^{22}, -4	3.9×10^{22}, -5

TABLE 8

VY CMa Model

Peak Monochromatic Luminosity, Velocity of Peak (ergs/s/Hz, km/s)

$\dot{M} = 1 \times 10^{-4}\ M_{\odot}/yr$

Transition		Without Dust	Dust Included
v = 0	J = 1 → 0	1.2×10^{25}, -31	2.1×10^{25}, -31
	J = 2 → 0	3.4×10^{24}, -31	7.6×10^{24}, -31
	J = 3 → 2	1.1×10^{23}, -29	2.2×10^{23}, -31
v = 1	J = 1 → 0	3.5×10^{20}, -8	2.1×10^{20}, -8
	J = 2 → 1	4.6×10^{22}, -8	3.8×10^{22}, -8
	J = 3 → 2	5.2×10^{22}, -8	4.3×10^{22}, -9

The most striking feature of the new profiles is the velocity structure. We see two distinct types of blueshifted peaks. The first originates inside R_o, in the slowly accelerating region, and has a velocity of -4 or -5 $km.s^{-1}$ for the Mira models and -8 or -9 $km.s^{-1}$ for the VY CMa model. The second originates far out in the maser region, very much like those seen in earlier models, and have velocities that are always close to the assymptotic velocity of the outflow. The vestigial remnants of the occulted red peaks are slightly more pronounced because of the larger size of the masing region in these models. Zero velocity peaks of maser emission are conspicuously absent from these models. Once again, the line widths are typically 2 - 3 $km.s^{-1}$. An example appears in Figure 6.

The line intensities for the Miras are comparable to those for the earlier $\epsilon = 1/2$ models, and slightly higher than those for the radiatively driven velocity law models. Since the inner region of the new models has the constant $\epsilon = 1/2$ property, this is not too surprising. Relative strengths of the various transitions follow the same patterns as before.

The effect of the dust on the line peaks appears, at first, ambiguous. The ground state masers in the $\dot{M} = 10^{-6}$ $M_\odot/yr$ model decrease in strength when the dust is added, but those of the other models all increase. The excited vibrational state masers all increase in luminosity with the addition of dust, except for the $v = 1$, $J = 1 \rightarrow 0$ line of the 5×10^{-6} $\dot{M}_\odot/yr$ model. The changes in

Figure 6. The v = 1, J = 3 → 2 transition from the $\dot{M} = 5 \times 10^{-6}$ $M_\odot$/yr Mira model, with dust included.

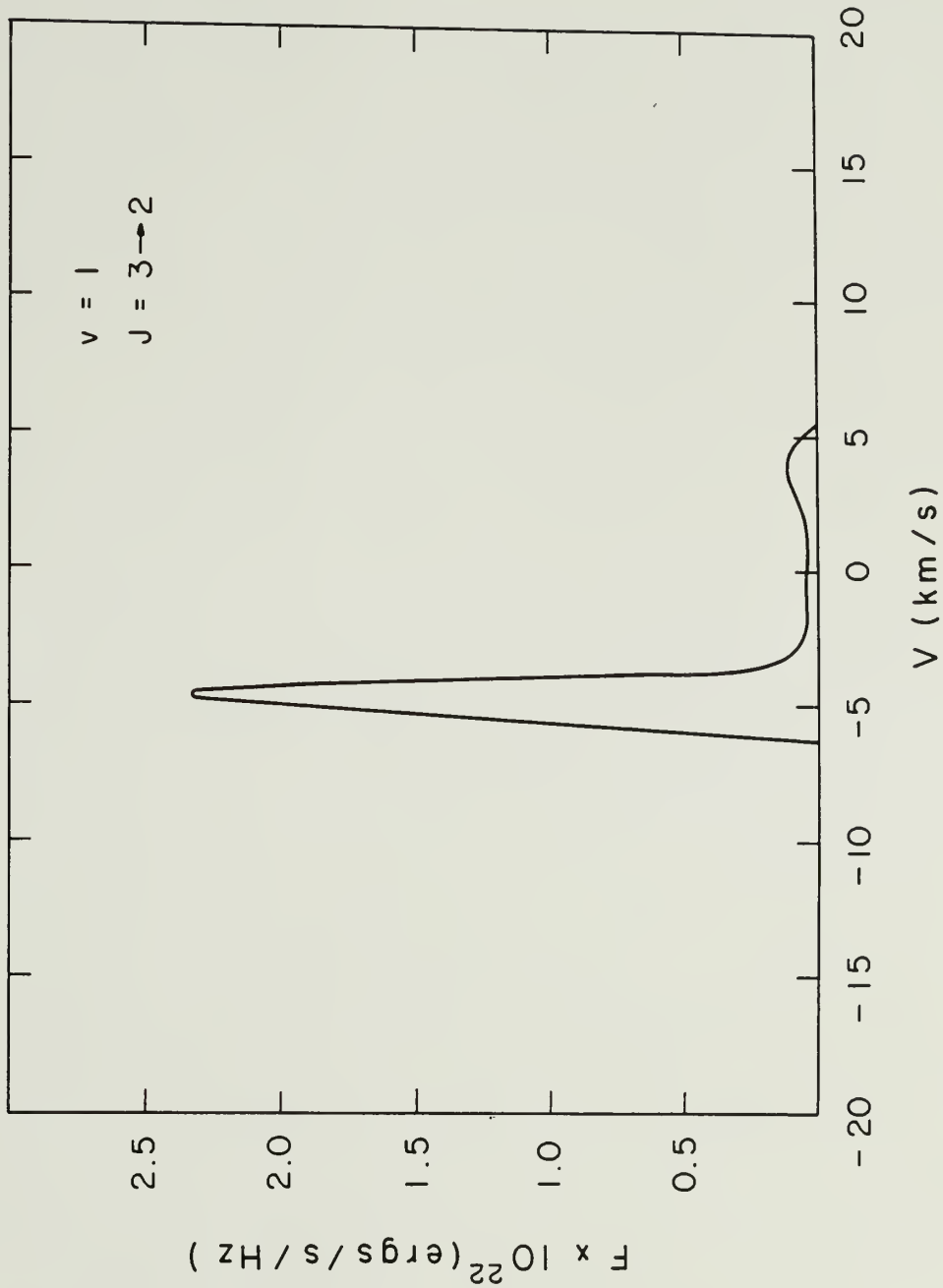
v = 1
J = 3→2
2.5
2.0
1.5
1.0
0.5
F x 10^22 (ergs/s/Hz)
-20
-15
-10
-5
0
5
10
15
20
V (km/s)

line luminosities with the addition of dust are always approximately equal to a factor of two or less.

Discussion

The most important inference from the results is the failure of the dust shell to make any significant qualitative changes. We have seen none of the possible changes in the pumping regions that the VY CMa data suggested, and those troublesome v = 0 masers still appear in the Mira models. All that seems to have occurred is a readjustment of the luminosities of the various transitions.

Let us consider the relative infrared fluxes in the maser region from the star and from the dust shell. The 8μ contribution of the shell must dominate that of the star in order to see any new effects, i.e.

$$\int_{-1}^{\mu_c} d\mu \; I_d \; \beta \gg \int_{\mu_c}^{1} d\mu \; I_* \; \beta \; . \tag{19}$$

All quantities are the same as previously defined. Inside the dust shell cavity, I_* is just the Planck function for the stellar disk, B_*. If $r \gg R_*$, we may approximate the stellar term,

$$\int_{\mu_c}^{1} d\mu \; I_* \; \beta \simeq 1/2 \; (1 - \mu_c) \; \beta_* \; (r) \; B_* \; .$$

Similarly, the dust term becomes

$$\int_{-1}^{\mu_c} d\mu \; I_d \, \beta \simeq I_d \, \bar{\beta} \; (r) \; .$$

Since the dust shells are thought to be, and indeed must be to reverse the anisotropy of the stellar radiation, optically thin at 8μ, we may approximate,

$$I_d = \int_{o}^{\tau_{max}} d\tau \; B_d \; (\tau) \; \exp \; (-\tau) \simeq \bar{B}_d \; \tau_{max} \; ,$$

where $\bar{B}_d$ is an average value for the dust's Planck function. Substitution yields

$$\tau_{max} \; B_d \; \bar{\beta} \gg 1/2 \; B_* \; \beta_* \; (1 - \mu_c) \; . \tag{20}$$

As you recall, $\bar{\beta}/\beta_*$ is one when the $\Delta v = 1$ transitions of the SiO are optically thin. In the optically thick limit,

$$\bar{\beta}/\beta_* = (2 + \varepsilon)/3\varepsilon \; .$$

In the pumping region, the 8μ lines are more thick than thin, so we adopt this limiting behavior. The conditions for the dominance of dust radiation can then be written,

$$\tau_{max} \gg 3\varepsilon \; B_* \; (1 - \mu_c)/[\bar{B}_d \; (4 + 2\varepsilon)] \; . \tag{21}$$

Not too surprisingly, this tells us that the dust shell is most important when ε is very small. That is to say, the lower limit on τ_{max} is smallest when ε is small, and is in fact proportional to ε

when $\varepsilon \ll 1$. Since a small value of ε implies a small acceleration, the optical depths in the stellar direction become much higher than those in the tangential. Hence, the tangential photons of the dust shell gain in relative importance. On the other hand, a large value of ε gives a constant lower limt for τ_{max}, in keeping with the smaller radial optical depths.

If we take parameters for the Mira model, we may estimate the lower limit of the dust shell's optical depth necessary for any significant effects to occur. Taking the maser region to be at 3 R_*, the average dust temperature to be 700K, we find limits of

$$\tau_{max} \gg 0.5 \text{ for } \varepsilon = 2 \text{ , and}$$

$$\tau_{max} \gg 0.2 \text{ for } \varepsilon = 1/2 \text{ .}$$

Since we have used an optical depth of 0.25 at 8μ, these criteria are clearly not met in our models. Even worse, they render very questionable the possibility of dust pumping by any optically thin shell.

Using the parameters for VY CMa, we find a similar result:

$$\tau_{max} \gg 0.1 \text{ for } \varepsilon = 2, \text{ and}$$

$$\tau_{max} \gg 0.05 \text{ for } \varepsilon = 1/2 \text{ .}$$

This assumes that the important maser region is just inside the dust shell's inner edge, and that the average dust temperature is 1000K. Since the model's shell depth is only 0.07 at 8μ, the lack of

significant dust effects is, again, consistent.

It is difficult to see how the 8μ optical depths of the Mira and VY CMa dust shells can be too much higher than the values we have used. Attempts to match the observed fluxes in optical and infrared inevitably lead to optical thinness at 8μ (e.g. Apruzese 1975). In any event, if the shells are not optically thin, then the anisotropy of the radiation from the dust must be reduced, since the path length would not be important. For a thick shell, a small anisotropy of dust infrared radiation would remain because of the dust temperature variation, in an effect analogous to limb darkening, but it is unlikely to be large.

The scattering of stellar infrared by the dust shell has been ignored in our calculations. The size of the scattering optical depth at 8μ is very uncertain since it depends strongly on the very poorly known size distribution of the dust grains. Even when the scattering is most important, the scattering optical depth is only comparable to that for the extinction (Apruzese 1975, Taam and Schwartz 1976). Therefore, even large back-scattering can change the infrared flux from the shell by no more than a factor of two or so, and our difficulties remain.

The only realistic way of making the dust pumping of our model more effective is to increase its average temperature. The dust temperatures at the inner edge of the shells in our models are already well above 1000K, so it is unlikely that the edge could be too

much hotter without evaporating the grains. An alternate way of increasing the average temperature is to move the average radius of the shell closer to the star without changing the optical depth. Unfortunately, a sharper fall-off in the opacity would require a mechanism for removing grains at larger radii, and would seem to be physically unrealistic. In fact, the models seem to indicate that the opacity distribution is closer to r^{-1} than to r^{-2} (Taam and Schwartz 1975), which makes the average dust temperature even lower. We can only conclude that the smooth, time-independent dust shell cannot produce the large effects we had hoped.

Another issue strongly related to the opacity distribution is the isotropy of the infrared flux, which is as important for radiative pumping as the total number of photons. At the inner edge of the r^{-2} dust distribution, the ratio of tangential to radial optical depths in the dust is

$$\tau_{max}\,(\mu = 0)/\tau_{max}\,(\mu = -1) = \pi/2\ . \qquad (22)$$

As the spatial thickness of the shell decreases, this ratio increases, and is infinite for the limiting case of an infinitely thin shell. Therefore, one can not only raise the average temperature, but also increase the anisotropy of the pumping radiation, if one can reduce the effective spatial thickness of the shell.

There are three distinct velocity regimes reflected in the line profiles of Tables 7 and 8, the inner $\varepsilon = 1/2$ region extending from

R_* to 1.1 R_o, the $\varepsilon > 1$ region extending from 1.1 R_o to 1.5 R_o, and the outer $\varepsilon < 1$ region extending from 1.5 R_o to infinity. The outer zone yields emission peaks at velocities near the assymptotic velocities, and the inner produces the peaks near -4 or -5 $km.s^{-1}$ for the Miras, and -8 or -9 $km.s^{-1}$ for VY CMa. Since $\varepsilon > 1$ in the middle zone, it would give rise to zero velocity peaks, but we find no significant maser emission from this region.

The mass loss rate determines the SiO number densities in the three regions, and, therefore, determines type of maser that may appear. With the lowest mass loss, ground state inversions take place in the inner zone, and no substantial excited vibrational state inversions occur. The larger mass loss rates push the $v = 0$ masers outward, and allow $v > 0$ masers in the inner zone. The velocities of the ground state peaks are, therefore, near v_∞, and those of the excited vibrational state masers nearer to zero. The densities in the outer $\varepsilon < 1$ region never become high enough to suppress the $v = 0$ masers in favor of the $v > 0$ in any of our models.

The absence of strong inversions in the central zone seems to be a consequence of the new velocity law. In the first place, this region is farther from the star than the $\varepsilon > 1$ region in earlier models; thus, the stellar radiation which is responsible for the pumping is more dilute. In addition, ε never becomes as large as in earlier models, drastically reducing the pumping efficiency. Finally, the maximum optical path is shorter in the middle zone because ε is

greater than one, as was discussed earlier.

We may ask whether the results show, at least to a small extent, some of the anticipated effects of dust shell pumping. After some investigation, the answer appears to be affirmative in all cases. A suppression of the anisotropic escape process is unambiguously responsible for the increased intensities of the v = 1 masers in the 5×10^{-6} $M_\odot$/yr and 1×10^{-5} $M_\odot$/yr Mira models, and for a decrease in the luminosities of the v = 0 masers in the 1×10^{-6} $M_\odot$/yr model. Note that all of these lines arise entirely within the inner velocity region of the envelope.

The increase in the luminosities of the v = 0 maser transitions of the two higher mass loss rate Mira models and the VY CMa model is not inconsistent with our expectations. Since these all originate in the outer part of the envelope, the majority of the dust's 8μ radiation comes from nearer the star, and simply reinforces the anisotropy of the stellar flux, rather than countering it. In a more realistic model, these masers would probably not exist at all, since they are well into the dust shell where a large portion of the SiO would be tied up in grains. A test run simulating 99% depletion of the SiO confirmed this idea, by showing no significant maser emission from the outer envelope.

Finally, the decrease in the v = 1 maser intensity with the addition of dust to the VY CMa model was found to be caused by a secondary effect of the dust shell. The increased amount of infrared

naturally raises the excitation temperature of the SiO, and changes the opacity in the $v = 1 \rightarrow 0$ pumping transitions. In the VY CMa model, this causes the region of strongest inversion to move farther from the star, moving it into the $\varepsilon > 1$ region where conditions are less favorable for inversions. The result is a truncation of the inversions with the subsequent lowering of line luminosity. The result can, therefore, tell us nothing about the anisotropic escape efficiency.

As an afterthought we attempted to produce a ground state inversion in the $\varepsilon > 1$ region by artificially reducing the stellar temperature. After taking T_* to be 500K, a weak inversion of the $J = 1 \rightarrow 0$, $v = 0$ transition appeared at the inner edge of the $\varepsilon > 1$ zone, but it persisted only to the inner edge of the dust shell. Total maser emission from that region was insignificant compared to outer envelope emission in the same transition.

Summary

Our main conclusions are:

1. The smoothly distributed dust shells modeled here cannot produce significant qualitative changes. Previous results from models without the shell remain valid.
2. The presence of the dust shell does lower the efficiency of the

anisotropic escape process.

CHAPTER VII

CONCLUDING REMARKS

We began this research with the aim of answering several rather clear-cut questions concerning SiO maser models. The easiest and, perhaps, most satisfying results concern the earlier work of Kwan and Scoville, and of Deguchi and Iguchi. We have been able to confirm the viability of both the radiative trapping and anisotropic trapping processes in our models and have, therefore, removed the doubts caused by some of the investigators' assumptions. In addition, we have established the conditions under which each of these mechanisms may be important, and how they interact. The model results cannot be completely reconciled with observations for the excited vibrational state masers, but the level of the inversions produced, particulary by the KS mechanism, certainly demonstrates that these processes must also operate in real circumstellar envelopes.

We have also presented and investigated the properties of a new mechanism, anisotropic escape. This was found to not only produce substantial inversions in the ground vibrational state of SiO, but also to strongly affect the pumping efficiency for masers in the higher vibrational bands. It is also a process which must be considered in any model expanding envelope.

The failure to find effects of the dust shell larger than a factor of two, of course, means that earlier work ignoring the dust

shell is still valid, but, unfortunately, it leaves open the questions concerning ground state masers. By juggling parameters, we were able to reduce the incidence of the ground state masers, but they always appeared to some extent in the models when the mass loss decreased. This has left us in the position of predicting ground state masers where they are not observed, and being unable to explain them when they are observed for VY CMa.

The most important consequence of this work may be the reinforcement of something we knew when we started. This is the fact that the maser lines are very sensitive to the velocity structure of the envelope. Yet that structure is very poorly known, and is usually assumed to follow some nice well-behaved function. As we have seen in our results, this assumption makes large qualitative and quantitative differences.

The obvious way that the velocity law influences the maser profiles is by setting their centers and widths. In this respect, maser emission is much like optically thin emission, since it probes the velocity and acceleration through the entire maser region. The average maser emission in our models is always blueshifted, whereas, real sources show a large fraction of redshifted emission (Lane 1982). This certainly indicates that our most reasonable choices of velocity law are not necessarily good descriptions of nature. In fact, the presence of the redshifted features in real spectra may well indicate infalling material in the inner maser regions, a situation which would

preclude time-independent models like ours.

We have also seen the way that the velocity structure changes the intensities and line centers of maser lines by controlling the types and efficiencies of the inversion mechanisms. Maser emission is unlike the optically thin in that the intensity grows exponentially with optical path length, making the intensity extremely sensitive to the velocity gradient. More importantly, the acceleration determines the relative importance of the anisotropic escape process which not only generates $v = 0$ masers, but also fixes the pumping efficiency of the radiative trapping mechanism for $v > 0$ masers. If, as we believe, radiative trapping is the dominant $v > 0$ inversion mechanism in the envelope, then the low maser power from our models suggests an error in our velocity law. The results of the arbitrary $\varepsilon = 1/2$ models show that maser luminosities comparable to those observed are possible with envelope models, and that a velocity law with large regions of intermediate acceleration (ε between 1/2 and 1) may more accurately describe the envelope.

Current models are clearly inadequate for describing SiO maser sources. As a result of this research, we do, however, have some suggestions for practical modifications that would alleviate some of the failings. Instead of abandoning spherical geometries, and their inherent simplicity, we hypothesize that time-dependent behavior plays a far more fundamental role in masers than had been thought.

All maser stars are variable in nature, a fact which can be

expected to have some direct influence on the SiO masers, if the stars contribute a substantial portion of the pumping photons. Indeed, correlation between maser luminosity and stellar light variations is frequently found (Lane 1982). It is also well known that SiO masers vary on time scales significantly shorter than those of the stellar light. However, these effects, and the mechanisms that produce them, are not as basic to the masers themselves as the type of time-dependent behavior needed to actually alter the character of the maser emission.

Our models indicate that the majority of the SiO maser region lies between the stellar photosphere and the inner edge of the circumstellar dust shell. When dust grains form, radiation pressure immediately accelerates them, and the associated envelope gas, producing the radiatively driven mass loss discussed earlier. Within the dust shell cavity, the maser region, there are indications that the mass loss is driven instead by shock waves (e.g. Hinkle et al. 1976). We suggest, on the basis of our work, that this mass loss must be episodic of sporadic, leading to large density variations (probably in the form of shells or portions of shells) within the SiO maser region. The observed maser profiles would then be a superposition of emission from the lumps of material, as indicated by VLBI observations (Lane 1982).

We have shown that there can be no large regions characterized by low values of ε where the maser emission arises; otherwise excited

vibrational state masers would not be as luminous as observed, and ground state masers would be prominent. Since the gas needs only to accelerate across thin shells, sporadic mass loss readily meets this requirement without the unobserved features discussed in Chapter V. It also allows for material which may fall back into the star, yielding redshifted emission, as indicated by observations (Lane 1982).

Another contradiction resolved by the "onion skin" structure concerns the locations of masers in different vibrational states. In Chapter IV we showed that, in general, these may never substantially overlap in the time-independent model; however, Lane has concluded, on the basis of similarities in velocity profiles and time variations, that $v = 1$ and $v = 2$ masers are in close proximity. Because of the large density variations over small changes of radius, the shell hypothesis not only allows this overlap, but requires it.

Recall that we were able to inhibit the anisotropic escape mechanism by juggling velocity parameters, and, thereby, reduce the luminosities of the ground state masers. They could not, however, be completely suppressed, unless one postulated a lower limit to the mass loss rate which seemed prohibitively high. In the context of the time-dependent model, only lower limits on the SiO number densities are required for the shells within the maser region. Once the dust forms, ϵ is greater than one for a considerable distance, forbidding $v = 0$ masers. Farther out in the envelope, too little SiO remains gaseous for masers. By considering shells and allowing material to

fall back into the star, total mass loss rates considerably smaller than the 10^{-5} $M_{\odot}$/yr discussed in earlier chapters could be reconciled with observations.

There are probably other effects associated with episodic mass loss, the magnitude of which can not easily be guessed. For example thin dust layers may be responsible for the v = 0 maser emission from VY CMa. Perhaps, turbulence generated when material is forced from the star also plays some role in the maser line formation. Answers to such outstanding questions and confirmation of our suggestions must wait for the completion of the next generation maser model.

BIBLIOGRAPHY

Andriesse, C.D. and Othof, H., 1973, Astr. and Ap., 27, 319.

Apruzese, J.P., 1975, Ap. J., 196, 753.

Bienick, R.J. and Green, S., 1982, preprint.

Buhl, D., Snyder, L.E., Lovas, F.J., and Johnson, D.R., 1975, Ap. J. (Letters), 201, L29.

Bujarrabal, V. and Ngu Yen-Q-Rieu, 1981, Astr. and Ap., 102, 65.

Cahn, J.H. and Elitzur, M., 1979, Ap. J., 231, 124.

Camy-Peyret, C. and Flaud, J.M., 1976, Mol. Phys., 32, 523.

Castor, J.I., 1970, M.N.R.A.S., 149, 111.

Clemens, D.P. and Lane, A.P., 1982, preprint.

Deguchi, S., 1980, Ap. J., 236, 567.

Deguchi, S., Good, J., Fan, Y., Mao, X., and Wang, D., 1982, preprint.

Deguchi, S. and Iguchi, T., 1976, Pub. Astr. Soc. Japan, 28, 307.

Dickinson, D.F., Reid, M.J., Morris, M., and Redman, R., 1978, Ap. J. (Letters), 220, L113.

Elitzur, M., 1980, Ap. J., 240, 553.

Geballe, T.R. and Townes, C.H., 1974, Ap. J. (Letters), 191, L37.

Goldreich, P. and Kwan, J., 1974, Ap. J., 189, 441.

Green, S. and Chapman, S., 1978, Ap. J. Supp. Series, 37, 169.

Hedelund, J. and Lambert, D.L., 1972, Ap. J. (Letters), 194, L71.

Hinkle, K.H., Barnes, T.G., Lambert, D.L., and Beer, R., 1976, Ap. J. (Letters), 210, L141.

Kwan, J. and Scoville, N.Z., 1974, Ap. J. (Letters), 194, L97.

Kwok, S., 1975, Ap. J., 198, 583.

Lane, A.P., 1982, Ph.D. Thesis, University of Massachusetts.

Lifshitz, A., 1974, J. Chem. Phys., 61, 2478.

Manson, E.L., Clark, W.W., DeLucia, F.C., and Gordy, W., 1977, Phys. Rev., 15, 223.

Merrill, K.M., 1977, I.A.U. Colloquium No. 42, The Interaction of Variable Stars with their Environment, ed. R. Kippenhahn, J. Rahe, and W. Strohmeier, p. 446.

Mihalas, D., 1978, Stellar Atmospheres (pub. W.H. Freeman and Co.).

Milikan, R.C. and White, D.R., 1963, J. Chem. Phys., 39, 3209.

Morris, M. and Alcock, C., 1977, Ap. J., 218, 687.

Olofsson, H., Rydbeck, O., Lane, A.P., and Predmore, C.R., 1981, Ap. J. (Letters), 247, L81.

Reimers, D., 1977, I.A.U. Colloquium No. 42, The Interaction of Variable Stars with their Environment, ed. R. Kippenhahn, J. Rahe, and W. Strohmeier, p. 559.

Schwartz, R.D., 1975, Ap. J., 196, 745.

Sherwood, W.A., Kreysa, E., and Schultz, G.V., 1977, I.A.U. Colloquium No. 42, The Interaction of Variable Stars with their Environment, ed. R. Kippenhahn, J. Rahe, and W. Strohmeier, p 434.

Snyder, L.E. and Buhl, D., 1974, Ap. J. (Letters), 189, L31.

Taam, R.E. and Schwartz, R.D., 1976, Ap. J., 204, 842.

Tipping, R.H. and Chackerian, C., 1981, J. Mol. Spect., 88, 352.

Townes, C.H. and Schawlow, A.L., 1955, Microwave Spectroscopy, pub. McGraw-Hill.

Tsuji, T., 1973, Astr. Ap., 23, 411.

Winnberg, A., 1977, I.A.U. Colloquium No. 42, The Interaction of Variable Stars with their Environment, ed. R. Kippenhahn, J. Rahe, and W. Strohmeier, p. 495.